AD-A178 237 AN ELF (EXTREMELY-LOW-FREQUENCY) TRANSMITTER EXPERIMENT 1/1
FOR THE SPACE SHU..(U) AEROSPACE CORP EL SEGUNDO CA
SPACE SCIENCES LAB H C KOONS 30 SEP 86
UNCLASSIFIED TR-0086(6940-06)-10-VOL-1 SD-TR-87-03-VOL-1 F/G 17/2.1 NL

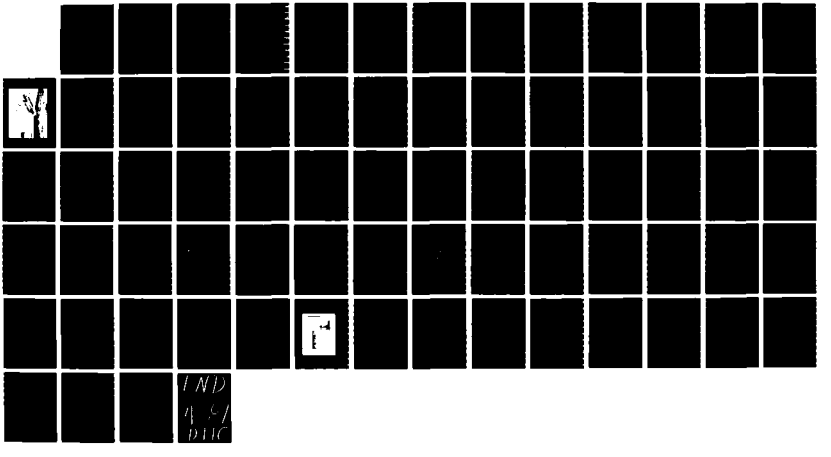

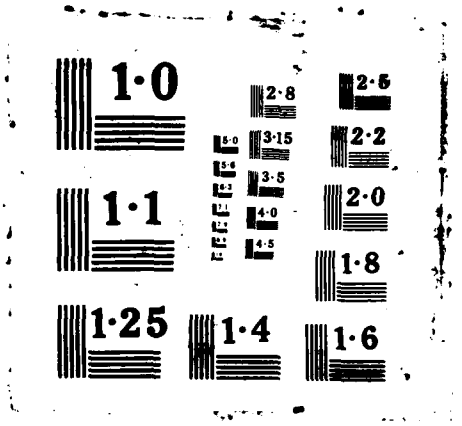
1·0
1·1
1·25
2·8
3·15
3·5
4·0
4·5
1·4
2·5
2·2
2·0
1·8
1·6

REPORT SD-TR-87-03

12

An ELF Transmitter Experiment for the Space Shuttle (The NASC-201 Experiment) Volume I

H. C. KOONS
Space Sciences Laboratory
Laboratory Operations
The Aerospace Corporation
El Segundo, CA 90245

30 September 1986

Prepared for
NAVAL AIR SYSTEMS COMMAND
Washington, D.C. 20361

SPACE DIVISION
AIR FORCE SYSTEMS COMMAND
Los Angeles Air Force Station
P.O. Box 92960, Worldway Postal Center
Los Angeles, CA 90009-2960

UNCLASSIFIED

SECURITY CLASSIFICATION OF THIS PAGE *(When Data Entered)*

REPORT DOCUMENTATION PAGE		READ INSTRUCTIONS BEFORE COMPLETING FORM
1. REPORT NUMBER SD-TR-87-03	2. GOVT ACCESSION NO. AD-A178237	3. RECIPIENT'S CATALOG NUMBER
4. TITLE *(and Subtitle)* AN ELF TRANSMITTER EXPERIMENT FOR THE SPACE SHUTTLE (The NASC-201 Experiment) Volume I		5. TYPE OF REPORT & PERIOD COVERED 6. PERFORMING ORG. REPORT NUMBER TR-0086(6940-06)-10
7. AUTHOR(s) Harry C. Koons		8. CONTRACT OR GRANT NUMBER(s) F04701-85-C-0086
9. PERFORMING ORGANIZATION NAME AND ADDRESS The Aerospace Corporation El Segundo, Calif. 90245		10. PROGRAM ELEMENT, PROJECT, TASK AREA & WORK UNIT NUMBERS
11. CONTROLLING OFFICE NAME AND ADDRESS Naval Air Systems Command Washington, D. C. 20361		12. REPORT DATE 30 September 1986 13. NUMBER OF PAGES 69
14. MONITORING AGENCY NAME & ADDRESS*(if different from Controlling Office)* Space Division Los Angeles Air Force Station Los Angeles, Calif. 90009-2960		15. SECURITY CLASS. *(of this report)* Unclassified 15a. DECLASSIFICATION/DOWNGRADING SCHEDULE

16. DISTRIBUTION STATEMENT *(of this Report)*

Approved for public release; distribution unlimited.

17. DISTRIBUTION STATEMENT *(of the abstract entered in Block 20, if different from Report)*

Same

18. SUPPLEMENTARY NOTES

19. KEY WORDS *(Continue on reverse side if necessary and identify by block number)*

ELF/VLF Transmitter
Ionosphere
Space Shuttle
VLF Communications

20. ABSTRACT *(Continue on reverse side if necessary and identify by block number)*

This report describes the design for a spaceborne elf/vlf transmitter. The transmitter could be used for experiments to obtain the radiation data in a space plasma required to determine the feasibility of an elf downlink communications system from a satellite to a subsurface antenna. The antenna is designed to be deployed by the Remote Manipulator Arm on the Space Shuttle.

DD FORM 1473 (FACSIMILE)

UNCLASSIFIED

SECURITY CLASSIFICATION OF THIS PAGE *(When Data Entered)*

CONTENTS

FIGURES

FIGURES (Continued)

TABLES

AN ELF TRANSMITTER EXPERIMENT FOR THE SPACE SHUTTLE (THE NASC-201 EXPERIMENT)

VOLUME I - SUMMARY

PREFACE

I wish to acknowledge and thank the following people who have contributed to the NASC-201 experiment design definition: C. Badcock, W. Chater, M. Dazey, W. Harbridge, C. King, R. Lott, P. Metzger and J. Roeder from Laboratory Operations. and M. Aswani, L. Bledjian, W. L. Butler, S. H. Chang, R. Crespo, F. B. Guo, J. D. Kawamoto, J. E. Kimble, R. B. Laube, H. G. Maier, C. J. Moening, G. A. Ozuna, O. A. Refling, T. W. Trafton and R. L. White, from the Engineering Group.

I also wish to thank H. Sampson, M. Neudorffer and E. Clark from the Space Test Program and Lt. W. Hampton from the Naval Space Systems Activity for their comments on the Statement of Work.

This is the final report on this project. The work was performed from FY81 through FY84. The information in this report is current to the end of FY84.

This work was supported by the Naval Air Systems Command and the U.S. Air Force Space Division under Contract No. F04701-85-C-0086.

BACKGROUND

The Naval Air Systems Command has provided support to The Aerospace Corporation for the mechanical and electrical design definition for an extremely-low-frequency (elf) space transmitter-receiver experiment based on a magnetic-dipole antenna concept. The system design was completed in FY84. This report documents the results.

EXPERIMENT OBJECTIVES

The primary objective of this experiment, known as NASC-201, is to test a spaceborne elf transmitter vehicle configuration capable of carrying out ionospheric elf missions. The experiment will obtain the elf radiation data in the space plasma required to determine the feasibility of an elf downlink communication system from a satellite to a subsurface antenna.

EXPERIMENT CONCEPT

To meet these objectives an experiment has been defined that consists of an elf transmitter facility aboard the Space Shuttle together with a subsatellite that is equipped with an elf receiver and environmental sensors. A magnetic dipole antenna has been chosen as the most suitable antenna for the transmitter. The antenna consists of 100 turns of 3/8 in. copper tubing supported by a structure approximately 134 in. in diameter and 81 in. long. It will be driven by a set of 12 power amplifiers in series to achieve an a.c. magnetic dipole moment of approximately 30,000 Amp-m2. The power budget is

Table 1. ELF Transmitter Power Budget

Power available	3000 watts
Conversion efficiency	0.85
Power to amplifiers	2550 watts
Amplifier efficiency	0.90
Power to antenna circuit	2295 watts

shown in Table 1. The transmitter will transmit signals at four frequencies: 500, 1000, 2000, and 4000 Hz. At these frequencies the radiation from the antenna is strongly controlled by the plasma environment. The radiation pattern bears no resemblance to the free-space radiation pattern for the same antenna. The elf receiver on the subsatellite will measure the intensity of the radiation as a function of distance from the antenna and as a function of the propagation direction of the signal with respect to the local geomagnetic field vector. The signal strength is axially symmetric about the direction of the local geomagnetic field vector. The separation between the Shuttle and the subsatellite will vary from approximately 10 km to 100 km over the mission. The concept is shown in Fig. 1.

The following measurements will be made on the subsatellite as part of the experiment: (1) Triaxial electric and magnetic field intensities at the elf signal frequencies, and (2) Single axis, wideband, electric and magnetic field intensities from 100 Hz to 20,000 Hz to determine the spectrum of the natural background emissions.

The following measurements are required from other experiments: (1) electron density and temperature, (2) dc vector magnetic field, and (3) ion composition and temperature.

The measurements are performed as follows: Before an elf transmission, all sensor parameters are recorded for at least five minutes to determine the background. The elf transmission is then initiated at a specified frequency, power level, and pulse pattern. The subsatellite will move through about a 45 deg portion of the antenna pattern in ten minutes. The elf receiver on the subsatellite will measure the intensity and propagation direction of the radiated signal. This sequence will be measured a sufficient number of times

Figure 1. The Experiment Concept

to cover the complete radiation pattern at all four frequencies at three distances.

A more detailed overview of the experiment is given in Appendix A, DD Form 1721, Space Test Program Flight Request for Experiment Number NASC-210, VLF Configuration Test.

RADIATION CALCULATIONS

Calculations of the radiation pattern and field intensity have been performed for several typical sets of ionospheric parameters. Figure 2 shows the field intensity at 1 kHz at a distance of 100 km from the antenna as a function of the polar angle of the radiated whistler-mode wave with respect to the geomagnetic field direction for the parameters listed in Table 2. The maximum signal intensity occurs at the inflection point in the index of refraction surface near a wave-normal angle of 60 deg where the wave normals are essentially parallel over a small angular range. In real space the energy propagates within a cone whose half-angle is approximately 20 deg.

These results have important implications for the conduct of the flight experiment. First, within the ionosphere the signal is only expected to be detected within an angle of about 20 deg with respect to the local magnetic field direction. There is adequate link margin to measure the field intensity to 100 km in the ionosphere. Second, the received wave field will consist of two components - one with a wave-normal angle below about 60 deg and one with a wave-normal angle above 60 deg. The one with the wave-normal angle above 60 deg will be an order of magnitude stronger than the one below 60 deg and thus will dominate the signal at the subsatellite VLF receiver. For transionospheric propagation the wave-normal angles near 60 deg are the most important

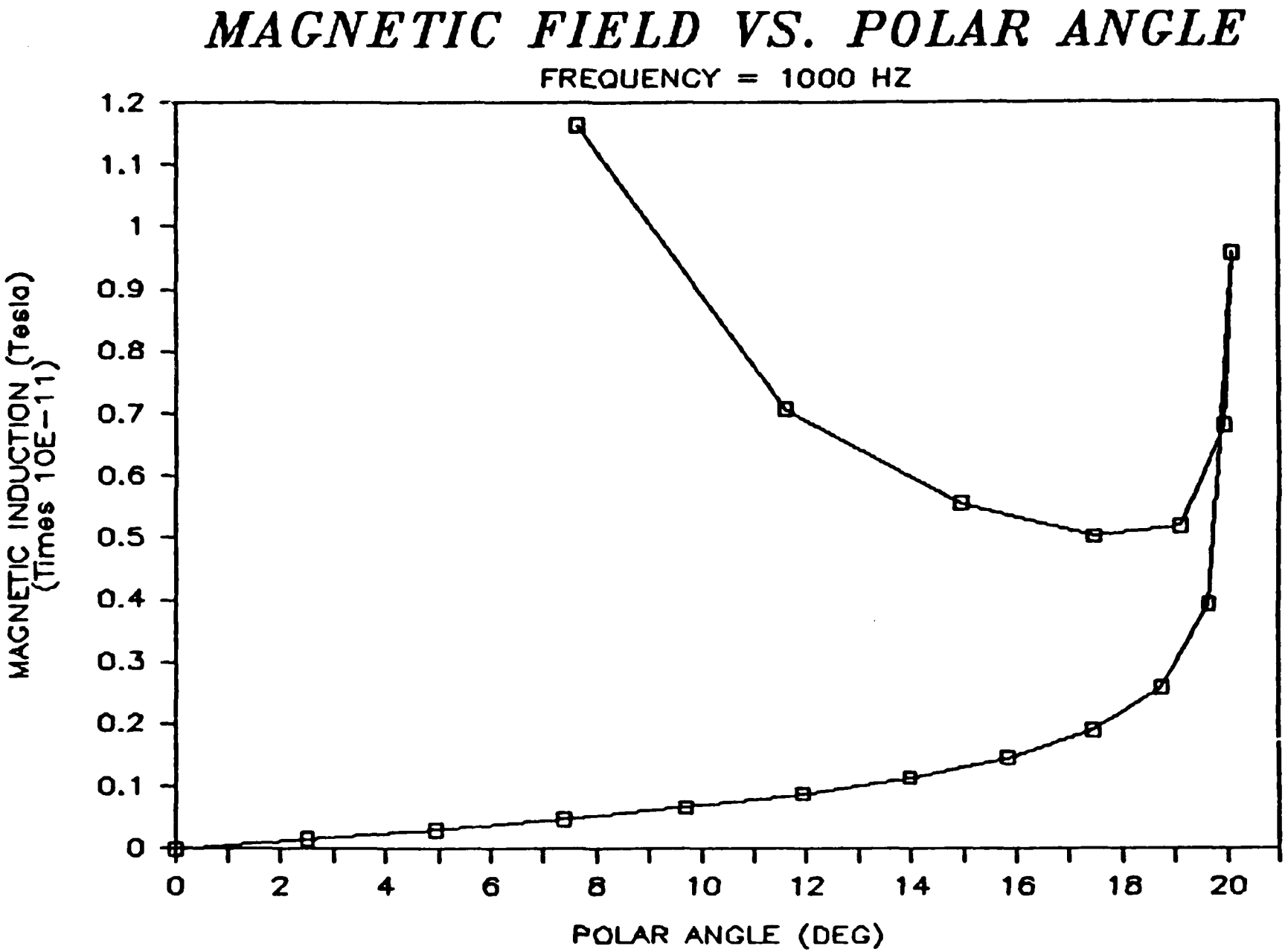

Figure 2. Radiated Field Intensity at a Distance of 100 km

Table 2. Ionospheric and Antenna Parameters used for the Radiation Calculations

IONOSPHERE	
Electron Density	2.4×10^6 cm^{-3}
Magnetic Field	0.428 Gauss
Ion Charge	1
Mass Ratio	16
Height of Ionosphere	90,000 m
ANTENNA	
Antenna Current	30 amps
Azimuthal Angle	0 deg
Antenna Radius	1.65 m
Turns	100
Distance	100,000 m
Magnetic Moment	25,659 amp-m^2

because they will produce the largest signal in the earth-ionosphere waveguide. An important objective of the flight experiment then is to measure the amplitude of this maximum which occurs near a wave-normal angle of 60 deg. In physical space this is at the edge of the group-velocity cone at an angle of about 20 deg with respect to the local magnetic field.

FUNCTIONAL OBJECTIVES

Functional objectives are used to plan a Space Shuttle mission timeline. They define what is to be done, where, and with what resources. Ten functional objectives have been defined for this experiment. They are listed in Table 3. The bulk of the time required to make the measurements is taken up by Functional Objective #5, Field intensity and antenna pattern measurements. That objective requires 32 hours of operations at the rate of about ten minutes per orbit. The functional objectives are defined in more detail in Appendix B.

EQUIPMENT

Four categories of equipment are required to perform the experiment:

First, an Antenna Structure subsystem has been defined to be deployed in space from the Space Shuttle cargo bay by the Remote Manipulator System and restowed for landing on conclusion of the experiment. The antenna structure supports copper tubing that comprises the magnetic dipole antenna. It also supports the experiment packages and power subsystem that make up the elf transmitter.

Second, a group of experiment packages has been defined to operate as an elf transmitter system in space. The experiment packages will be integrated onto the antenna structure. They will drive an a.c. current at elf through the copper coils of the antenna structure.

Table 3. NASC-201 Functional Objectives

FO No.	Title
1.	Transmitter systems start up
2.	Checkout transmitter at low power
3.	Unstow and deploy transmitter
4.	Checkout deployed transmitter at high power
5.	Field intensity and antenna pattern measurements
6.	Ground reception of signal
7.	Restow transmitter
8.	Transmitter system shutdown
9.	B-field meter turn on
10.	B-field meter turn off

Third, two instruments have been defined that remain in the cargo bay. These are a Data Interface Unit and a B-field meter. The Data Interface Unit is a command and telemetry interface between the orbiter and the experiment packages on the antenna structure. The B-field meter will remotely monitor the current in the antenna by measuring the magnetic field at the signal frequency in the cargo bay.

Fourth, an elf/vlf receiver and a six axis antenna system has been defined for a subsatellite to measure the signals transmitted by the elf transmitter.

The experiment packages and the Antenna Structure are described in detail in the next sections.

A Statement of Work that delineates a contractor's effort required to design, analyze, develop, fabricate and test an elf transmitter for this experiment is contained in Volume II of this report.

Experiment Packages

A block diagram of the transmitter system is shown in Figure 3. The following experiment packages make up the transmitter system:

Data Unit. The Data Unit will receive commands via existing cables along the RMS from a Data Interface Unit in the cargo bay. It will send commands to the other experiment packages. It will collect measurements from the other experiment packages, format the data, and transmit the data to the Data Interface Unit via the existing cables along the RMS.

The Data Unit and the Data Interface Unit are two identical packages, one located on the Antenna Structure, the other within the cargo bay. Each package will accomplish its different functions using an 8344 microcontroller-based

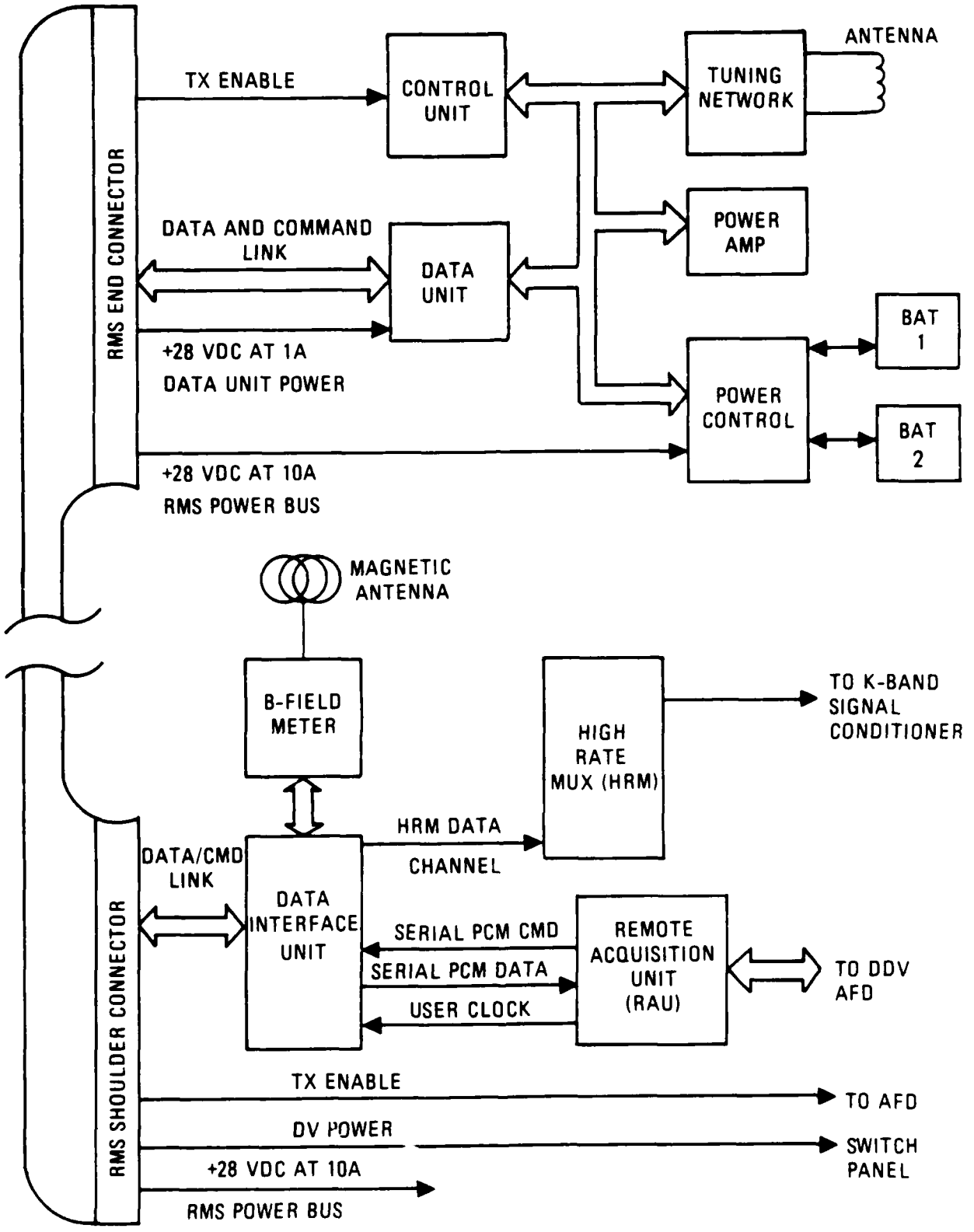

Figure 3. A Block Diagram of the Transmitter System

design that provides general purpose programming flexibility for data processing, for input/output control, and for serial communication between the two units. Analog to digital converters will augment the basic digital design to condition the many analog signals, such as the current, voltage, and temperature measurements, for digital processing.

The digital nature of the memory and communications functions dictate the necessity for a general programmable logic structure as opposed to a random logic design.

Considerable investigation was made into the feasibility of using a commercial "shuttle-qualified" computer, the SC-1 from Southwest Research Institute. It was determined that performance and cost exceeded the requirements for this experiment. It also lacked the capability to communicate between the two units.

Other alternatives were also examined. Various LSI-11 commercial board implementations as well as uJ-11 chip-based board designs were considered. These were attractive because of considerable in-house experience and development capability. The relatively high power dissipation and questionable quality control were negative factors that weighed against this approach.

Various other microprocessor and microcontroller-based board designs were seriously considered involving the following family of devices: NSC800, i8048, i8051, and i8096. Any of these could be acceptable with some reservations regarding sufficient product maturity of the 8096.

Along with the various designs, corresponding effort was expended in the study of suitable development system support. This was especially true for the SC-1 computer that involved the tri-processors 8086, 8087, and 8089 and also the 8571.

The design based on the i8344 has been chosen and an enhanced Intel iPDS100 development system has been purchased using Aerospace Capital Budget funds to assist in the development of the data units. The data units can be built in small packages because of the high level of functional integration in the i8344 chip. The size is set by the connectors required for input/output.

Since the data unit packages will have considerable space available, some effort has been devoted to the conceptual design of internal reconfigurations to permit experiment modification and or enhancements without the necessity for interior access. This would, for example, allow reprogramming after the units have been installed.

Figure 4 shows the outline and mounting drawing for the Data Unit based on the i8344 design.

Control Unit. The control unit will provide square waves to drive the twelve power amplifiers and a sine wave to measure the resonant frequency of the tuned antenna circuit.

Figure 5 shows a schematic diagram of the functions of the control unit in the NASC-201 experiment. The control unit contains a crystal oscillator and frequency synthesizer and a 50 watt sine-wave power amplifier to measure the resonant frequency of the tuned antenna circuit.

This amplifier will put a constant voltage sine-wave signal into the load at its resonant as well as its non-resonant frequencies. The circuit consists of a single feedback loop with a low-level operational amplifier chip driving a linear push-pull output stage. The P and N channel output driver transistors are "Hexfet" power transistors capable of supplying up to 20 amps peak current. They are driven by an npn-pnp pair in a local feedback loop which fixes a gain of 10 in the output stage. The power source for the amplifier is ± 12 volts at up to six amps, supplied by a power inverter circuit.

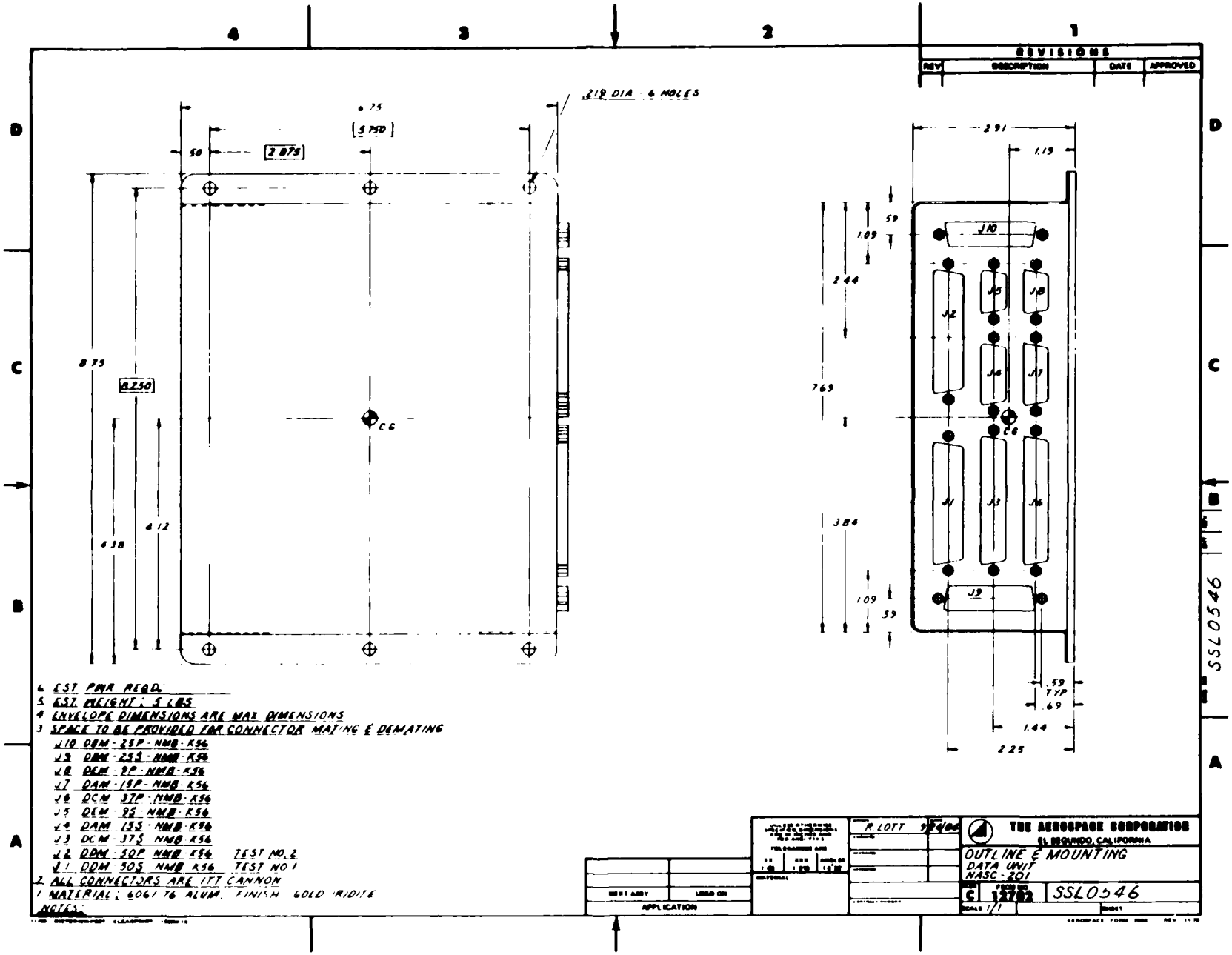

Figure 4. The Outline and Mounting Drawing for the Data Unit Based on the i8344 Design

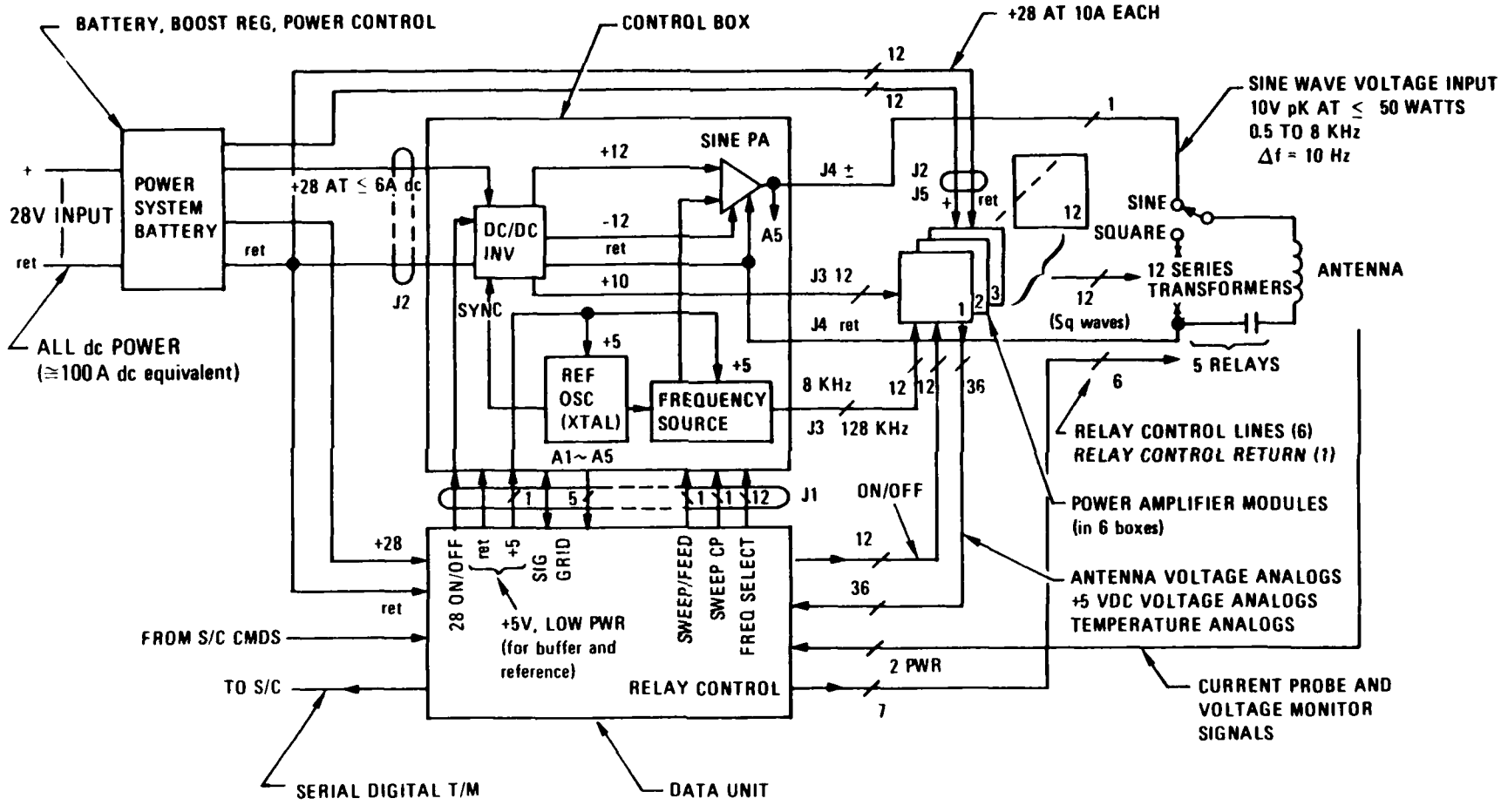

Figure 5. A Schematic Diagram of the Functions of the Control Unit

The Control Unit also provides the frequency source and control signals to drive the 12 square-wave power amplifiers in the elf transmitter. All logic in the control unit will be CMOS logic.

Figure 6 shows the outline and mounting drawing for the Control Unit.

Power Amplifiers. There are twelve power amplifiers housed in pairs in six enclosures. The power amplifiers are connected in series and provide the primary signal for the magnetic antenna. The amplifiers form a set of series-connected square-wave drivers which are intended for use only at the series-resonant frequencies of the antenna. The square-wave amplifier circuit makes use of a multiple of small N and P channel "Hexfet" power transistors paralleled to make a very low ON switch resistance. The circuit is a bridge with the load being the primary of the output transformer. The ends of this primary are switched alternately to ground and to the input power supply value, nominally +25 volts. Logic levels of 10 volts drive the bridge circuit, a d provide a balanced drive timing with a delay included to prevent overlap of the ON states of the power transistors. The logic also includes automatic shutdown in case of the loss of the input timing pulses. An on-off control bit can cause the amplifier to go into an inactive mode, so that its contribution to the total signal is reduced to only a diode drop. Input signals and a voltage analog output are transformer coupled so as to provide ground isolation of this high-power system, which could develop sizable voltage drops in the signal return leads.

Figure 7 shows the circuit design schematic for one of the power amplifier modules.

Figure 8 shows the outline and mounting drawing for a Power Amplifier Unit. Each unit contains two power amplifier modules.

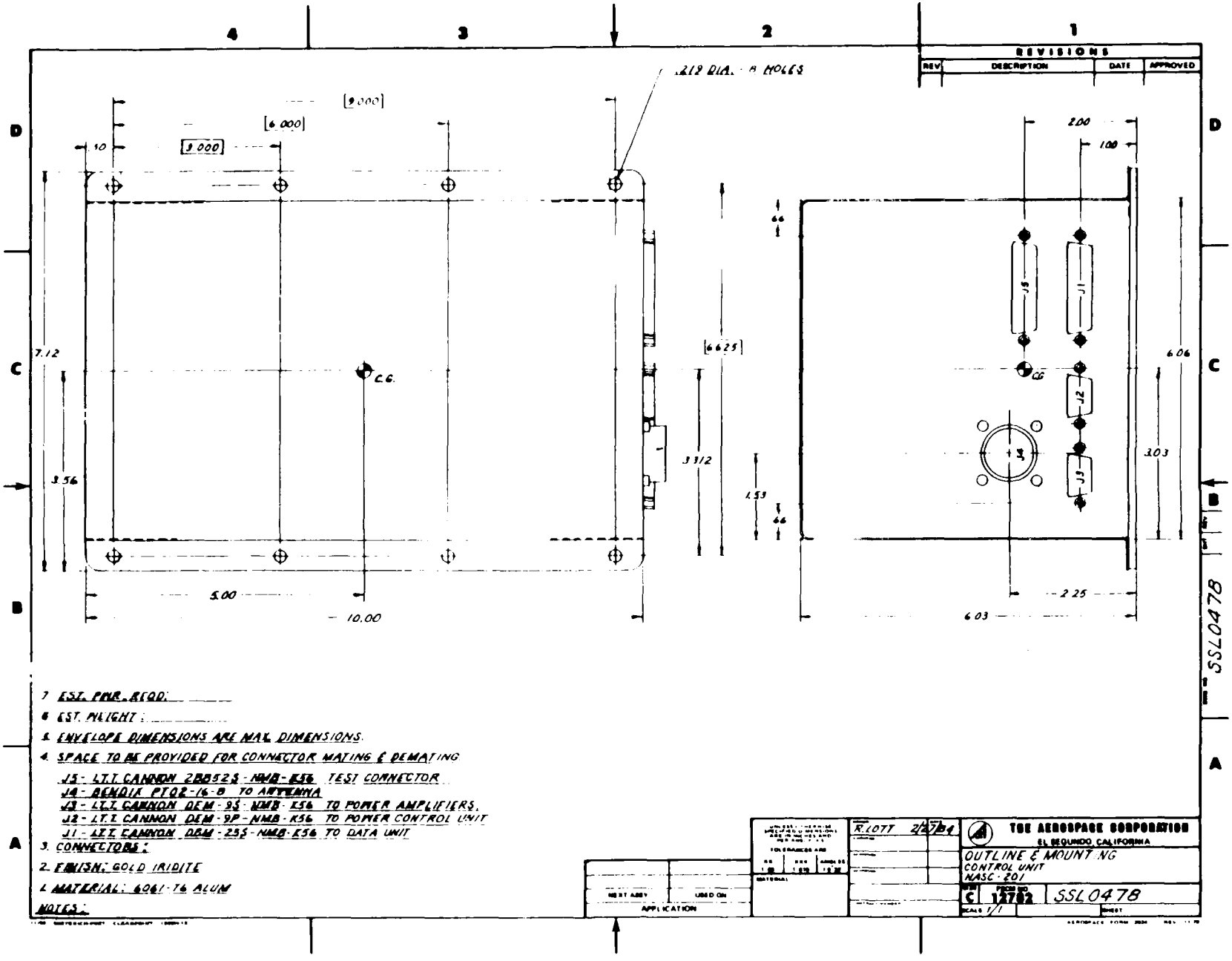

Figure 6. The Outline and Mounting Drawing for the Control Unit

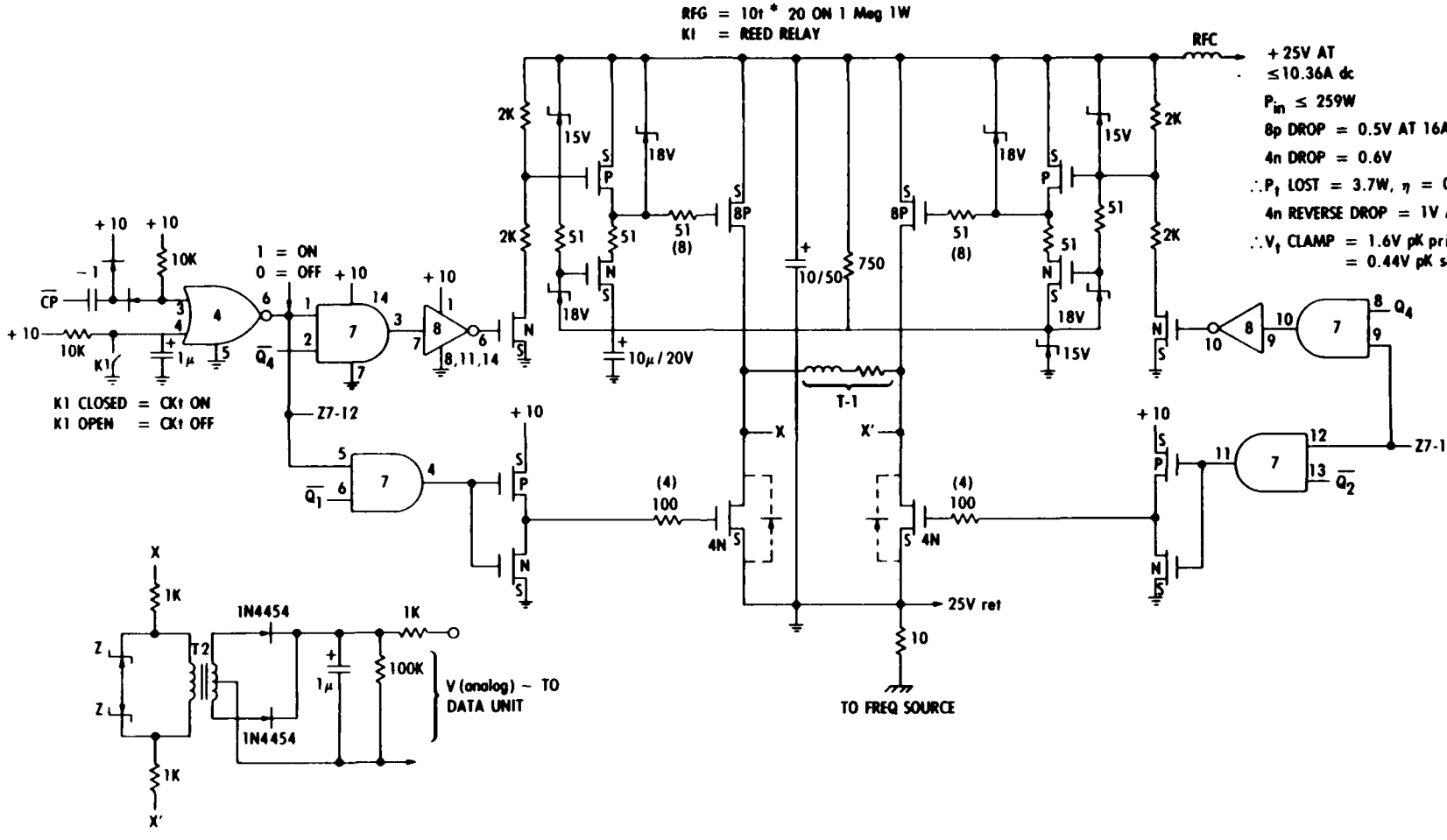

Figure 7. The Circuit Design Schematic for One of the Power Amplifier Modules

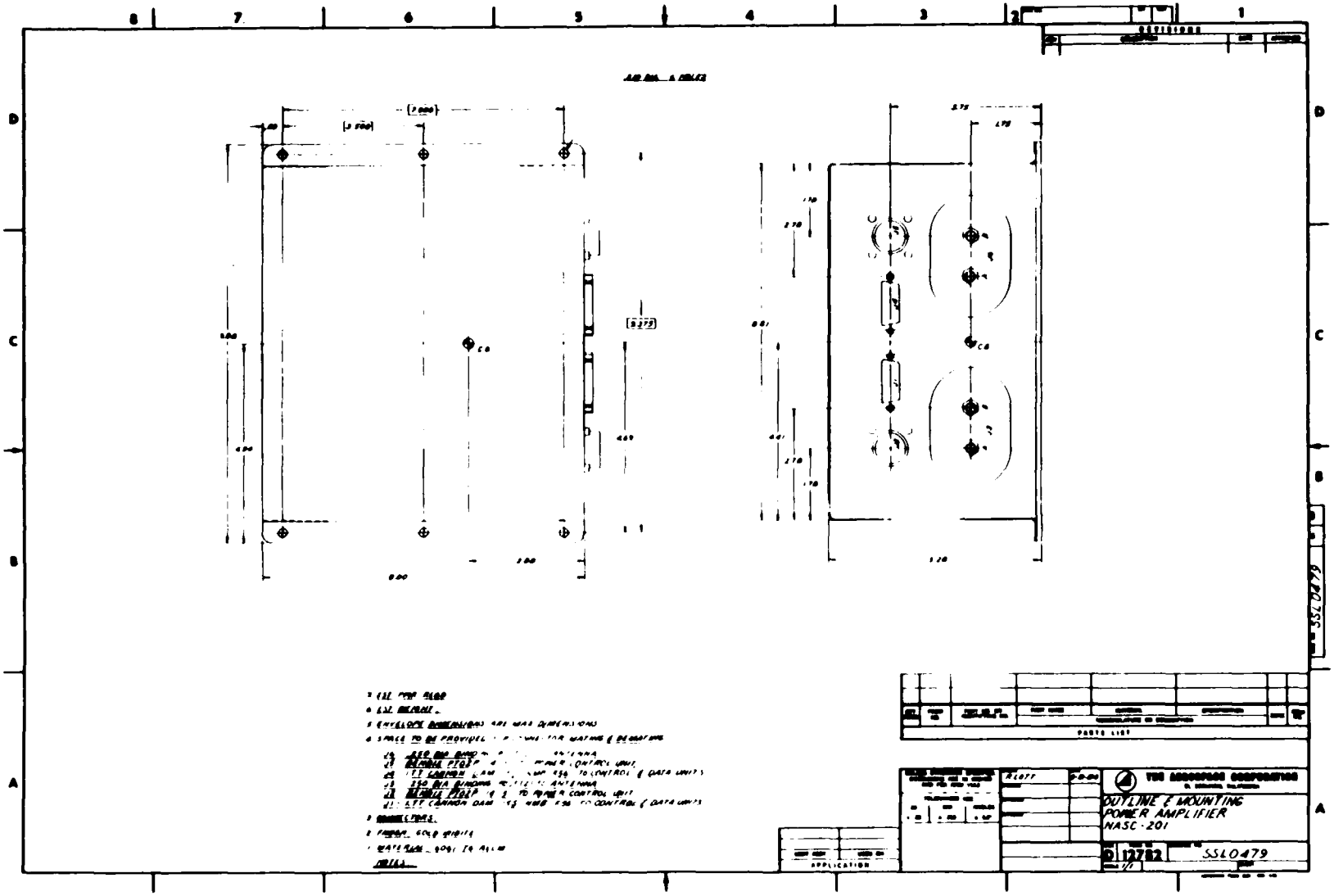

Figure 8. The Outline and Mounting Drawing for a Power Amplifier Unit

Tuning Network. The NASC-201 antenna circuit is a simple series-resonant inductive-capacitive (LC) circuit. It is planned to operate the transmitter at four frequencies, 500, 1000, 2000, and 4000 Hz. The simplified tuning circuit diagram is shown in Fig. 9.

There are eight capacitor units that can be connected in various series and parallel combinations to tune the antenna circuit. A voltage divider unit divides down the high-voltage a.c. signal across the capacitors to provide a low level signal of the voltage waveform to the Data Unit for processing. A current probe provides a low level signal of the antenna current waveform to the Data Unit for processing. The circuit includes six high-voltage switches. Two switch between the square-wave and the sine-wave source and four switch the capacitor units into and out of the circuit.

The four frequencies were chosen to allow capacitor values and voltages to be obtained from combinations of identical capacitors to reduce the costs that might be encountered if four different capacitors were required. Two types of capacitors, high voltage and low voltage, are required.

Most of the energy in the circuit will be dissipated in the antenna coil. Since the system has a high Q, the voltage will be quite large across the capacitors. Therefore, depending upon the dissipation factor or equivalent series resistance (ESR) of the capacitors, there will be considerable power dissipation in the capacitors. The requirements for capacitors for this experiment are sufficiently unique that no commercial source has been found to provide them.

Several possible approaches have been considered. First, a contract might be awarded for the design, development, manufacture and testing for the capacitors. Second, companies with capabilities to construct non-flight capacitors

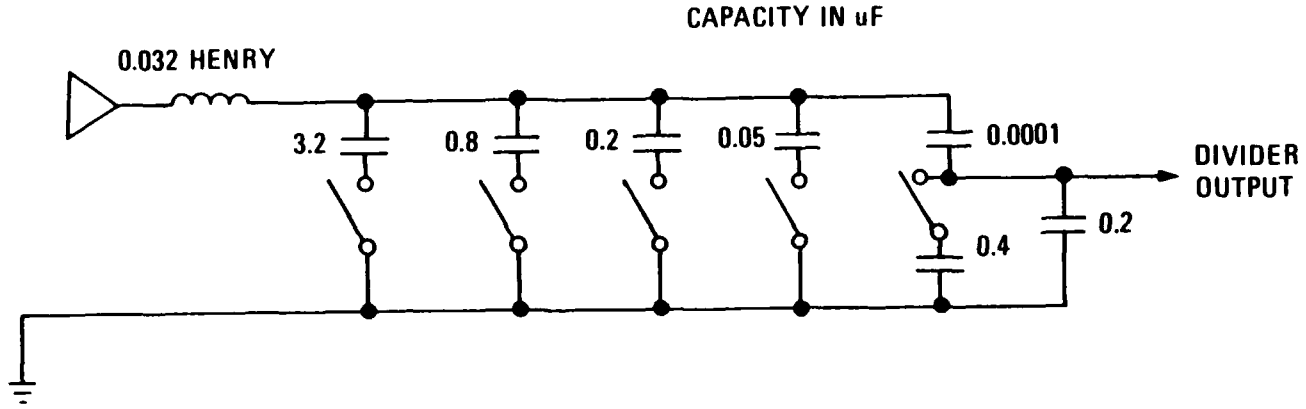

Figure 9. A Simplified Diagram of the Tuning Circuit

with the necessary requirements might be involved in a joint effort to produce the flight capacitors. We are persuing both courses at this time and can not yet make a recommendation as to the one to follow.

Figure 10 shows the outline and mounting drawing for a Capacitor Unit. There are eight such units. Figure 11 shows the outline and mounting drawing for the Voltage Divider Unit.

The specific requirements for the capacitors are listed in Appendix C.

RMS Interface. The NASC-201 antenna is electrically linked to the shuttle orbiter via the cable running the length of the Remote Manipulator System (RMS). The connection to the antenna is made through the Special Purpose Electrical Connector in the Standard End Effector. Figure 3 is a block diagram of the NASC-201 experiment. The top half of the figure shows the various antenna subsystems and their connection to the RMS end effector. The bottom half of the figure shows the part of the experiment that is mounted on the pallet and the interface to the Spacelab subsystems. All data and commands are transferred to and from the antenna via a bi-directional synchronous digital channel. Two hundred and eighty watts of power are provided by the RMS power bus to trickle charge the silver-zinc batteries. The Data Unit is powered separately by redundant paths controllable from a switch panel on the Aft Flight Deck (AFD). The switch panel will also have a hardwired safing command named 'Tx Enable' to control the antenna high-power systems. All other commands and some minimal engineering data will be routed through the Spacelab serial PCM links to the Data Display Unit (DDU) on the Aft Flight Deck. All data will be sent to the ground through the High Rate Multiplexer System.

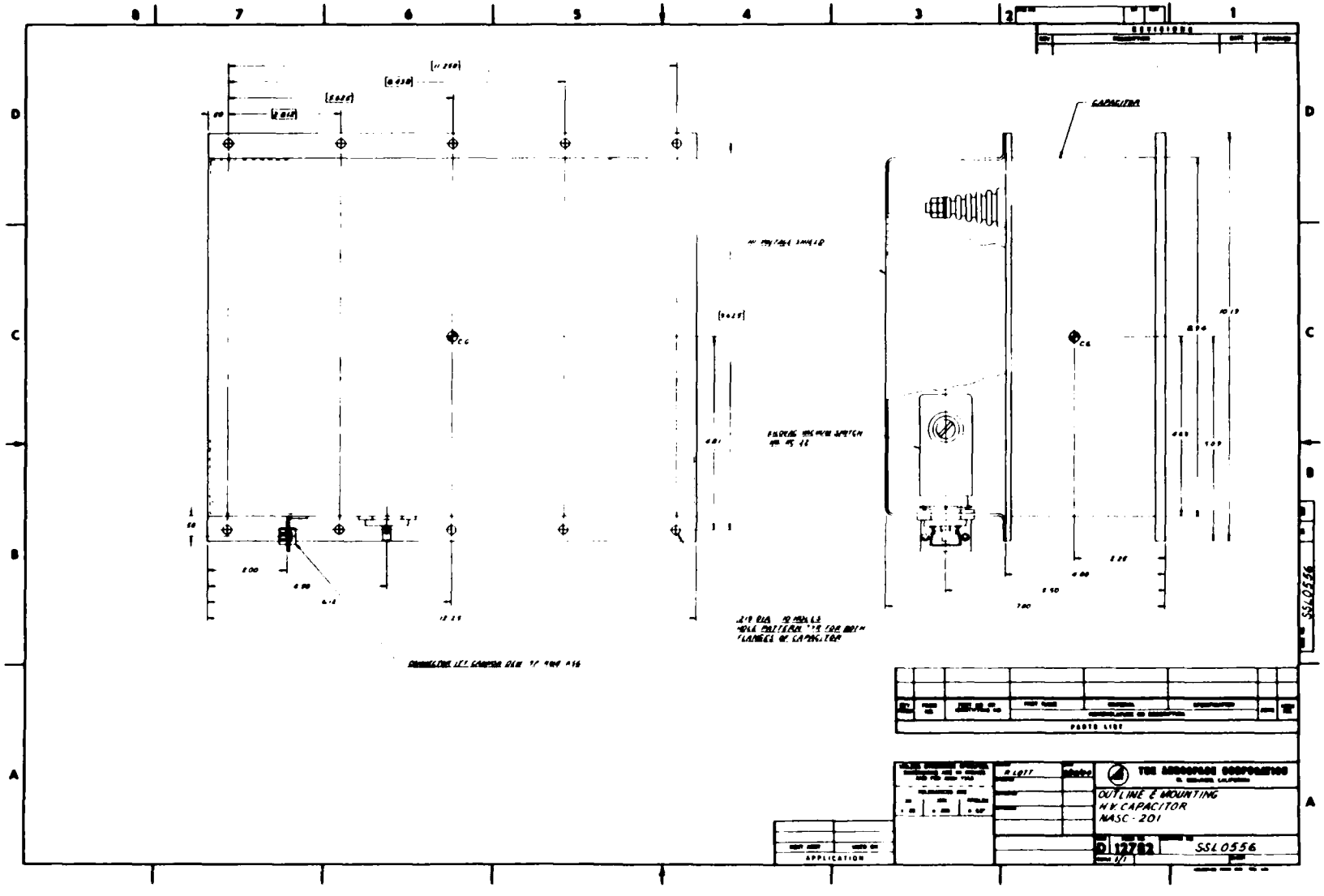

Figure 10. The Outline and Mounting Drawing for a Capacitor Unit

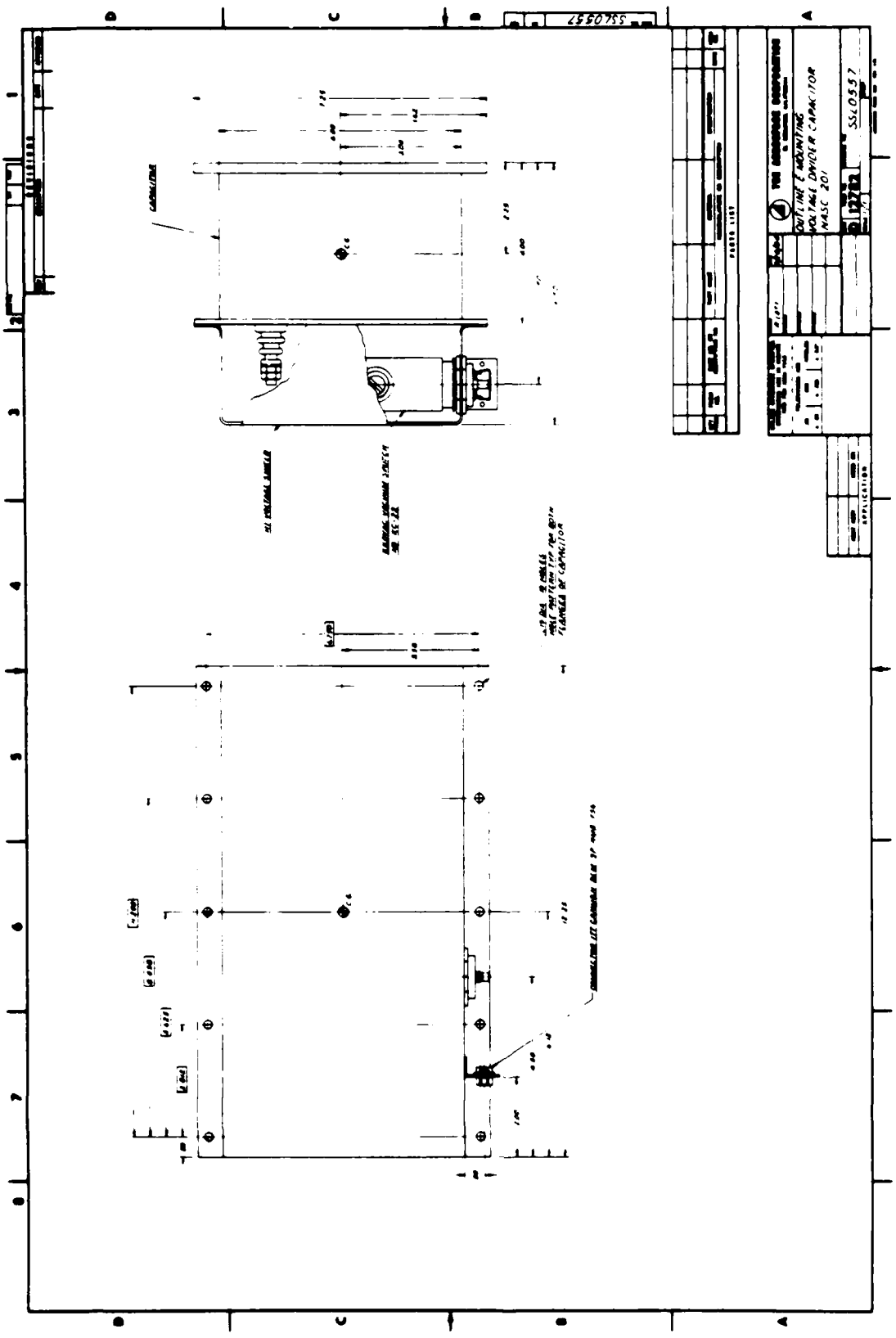

Figure 11. The Outline and Mounting Drawing for the Voltage Divider Unit

Data Requirements. Preliminary data requirements for the Data Interface Unit are given in Table 4. Preliminary command requirements for the Data Interface Unit are given in Table 5.

Mechanical Design and Mass Properties. The dimensions and weights of the individual items making up the experiment packages are listed in Table 6. The mechanical interfaces and experiment package outline and mounting drawings are shown in Figs. 4, 6, 8, 10, and 11. All experiment package dimensions and weights are preliminary. They are best estimates based on the present state of the definition of each package.

We have assigned a not-to-exceed weight of 300 lbs to the experiment packages for the purpose of obtaining the mass properties of the entire antenna structure.

Interconnection Diagrams. There are five different types of electrical circuits comprising the elf transmitter: data, control, power subsystem, low level power (logic), and the antenna current. Figures 12 to 16 show the package interconnection diagrams for each type of circuit.

Wiring lists for each of the experiment packages is given in Appendix D.

Antenna Structure

The antenna structure is shown in Fig. 17. It consists of a cylindrical honeycomb structure 134 in. I.D. x 137 in. O.D. x 81 in. long. Attached to the O.D. of the honeycomb cylinder is a "hat" section ring frame consisting of five pieces; two honeycomb sections, two longeron/equipment mounts, and a keel trunnion mounting structure. The electrical power equipment, experiment packages, cabling, and trunnions are mounted to the ring frame. The Flight

Table 4. Data Requirements

Measurement	Type	Sample Rate	Bits/ Word	Bits/ Sec
Amplifier Control Unit:				
Chill Plate Temp	0-5 VDC	1/sec	8	8
Voltage Monitor 1	0-5 VDC			
Voltage Monitor 2	0-5 VDC			
Voltage Monitor 3	0-5 VDC			
Sine Wave Volt RMS	0-5 VDC	TBD	8	8
Sweep/Fix	Bi-Level	1/sec	1	1
Frequency Code	Digital	TBD	12	TBD
Housekeeping	TBD	TBD	TBD	TBD
Power Amplifier (12):				
Control Bit (12)	Bi-Level	1/sec	1	12
Trans Primary Volt (12)	0-5 VDC	TBD	8	TBD
+5 Volt DC Monitor	0-5 VDC			
Chill Plate Temp (12)	0-5 VDC	1/sec	8	96
Voltage Monitor +28 V (12)	0-5 VDC	1/sec	8	96
Housekeeping	TBD	TBD	TBD	TBD
Capacitor (8):				
Temperature (8)	0-5 VDC	1/sec	8	96
Voltage Divider Unit:				
Capacitor Voltage, VC	0-5 VDC	40,000/sec	8	320,000
Temperature	0-5 VDC	1/sec	8	8
Current Probe:				
Antenna Current, Ia	0-5 VDC	40,000/sec	8	320,000
Temperature	TBD	TBD	TBD	TBD
Data Unit:				
Housekeeping	TBD	TBD	TBD	TBD
Battery:				
TBD	TBD	TBD	TBD	TBD
Power System:				
TBD	TBD	TBD	TBD	TBD
Antenna:				
Temperature (8)	0-5 VDC	1/sec	8	64
Total Amplifier Volt, Vt	0-5 VDC	TBD	TBD	TBD

Table 5. Command Requirements

Command	Bits
Frequency Code	12
Sweep/Fix	1
Pwr Amp on/off	12
Pulse Period	TBD
Pulse Duration	TBD
Switch Configuration	6
Power Distribution	TBD
Select Program	TBD

Table 6. Experiment Package Dimensions and Weights

Item Number	Item Name	Dimensions In	Weight lbs
DU	Data Unit	7 x 9 x 3	5
CU	Control Unit	7.2 x 10 x 6	5
CP	Current Probe	TBD	TBD
VD	Voltage Divider Unit	12.3 x 6.8 x 6.5	TBD
PA-A	Power Amplifier Unit A	8 x 10 x 5.3	12
PA-B	Power Amplifier Unit B	8 x 10 x 5.3	12
PA-C	Power Amplifier Unit C	8 x 10 x 5.3	12
PA-D	Power Amplifier Unit D	8 x 10 x 5.3	12
PA-E	Power Amplifier Unit E	8 x 10 x 5.3	12
PA-F	Power Amplifier Unit F	8 x 10 x 5.3	12
CAP-1	Capacitor Unit 1	10 x 12 x 7	17
CAP-2	Capacitor Unit 2	10 x 12 x 7	17
CAP-3	Capacitor Unit 3	10 x 12 x 7	17
CAP-4	Capacitor Unit 4	10 x 12 x 7	17
CAP-5	Capacitor Unit 5	10 x 12 x 7	17
CAP-6	Capacitor Unit 6	10 x 12 x 7	17
CAP-7	Capacitor Unit 7	10 x 12 x 7	17
CAP-8	Capacitor Unit 8	10 x 12 x 7	17
SW-1	Switch 1	TBD	TBD
SW-2	Switch 2	TBD	TBD
SW-3	Switch 3	TBD	TBD
SW-4	Switch 4	TBD	TBD
SW-5	Switch 5	TBD	TBD
SW-6	Switch 6	TBD	TBD

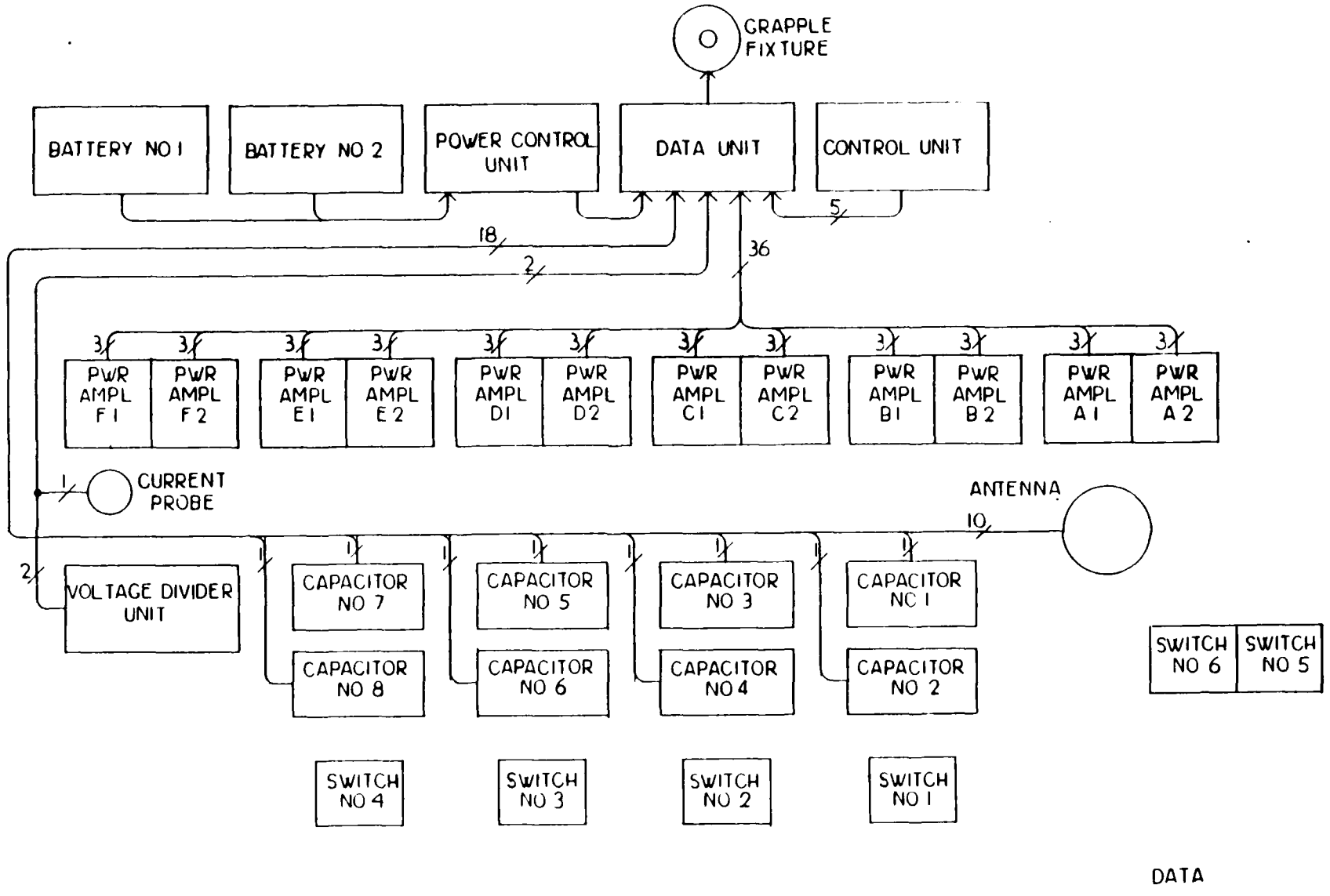

Figure 12. The Package Interconnection Diagram for the Data Circuits

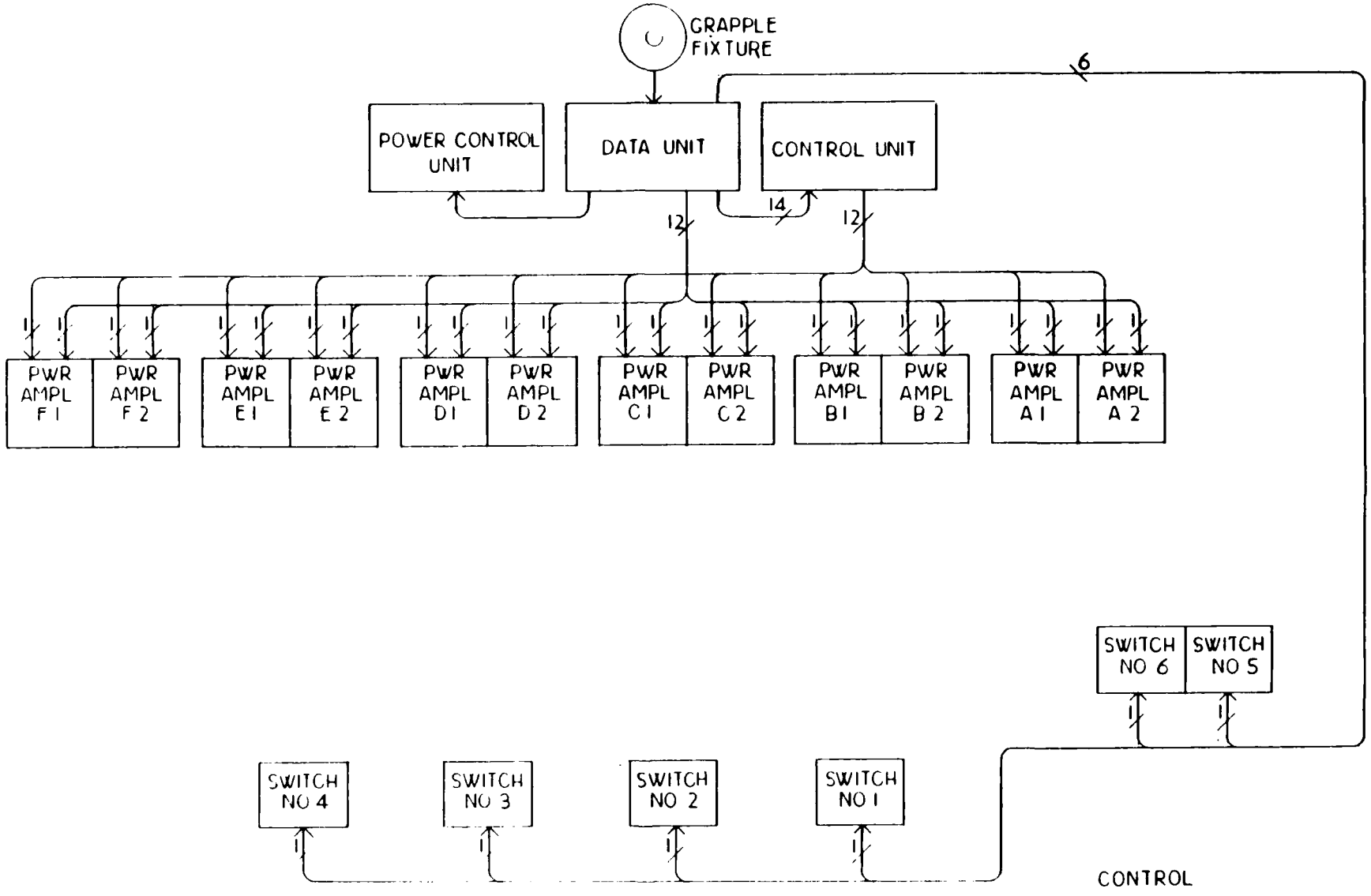

Figure 13. The Package Interconnection Diagram for the Control Circuits

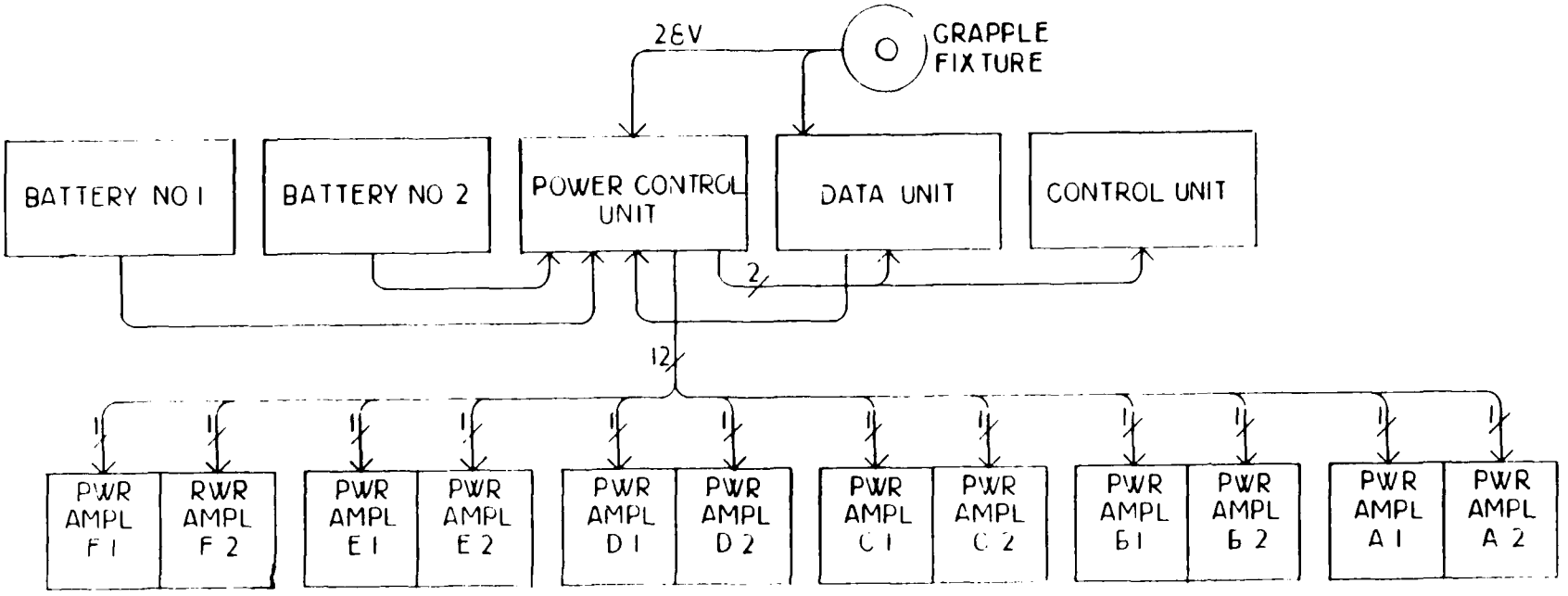

POWER SUB-SYSTEM

Figure 14. The Package Interconnection Diagram for the Power Subsystem Circuits

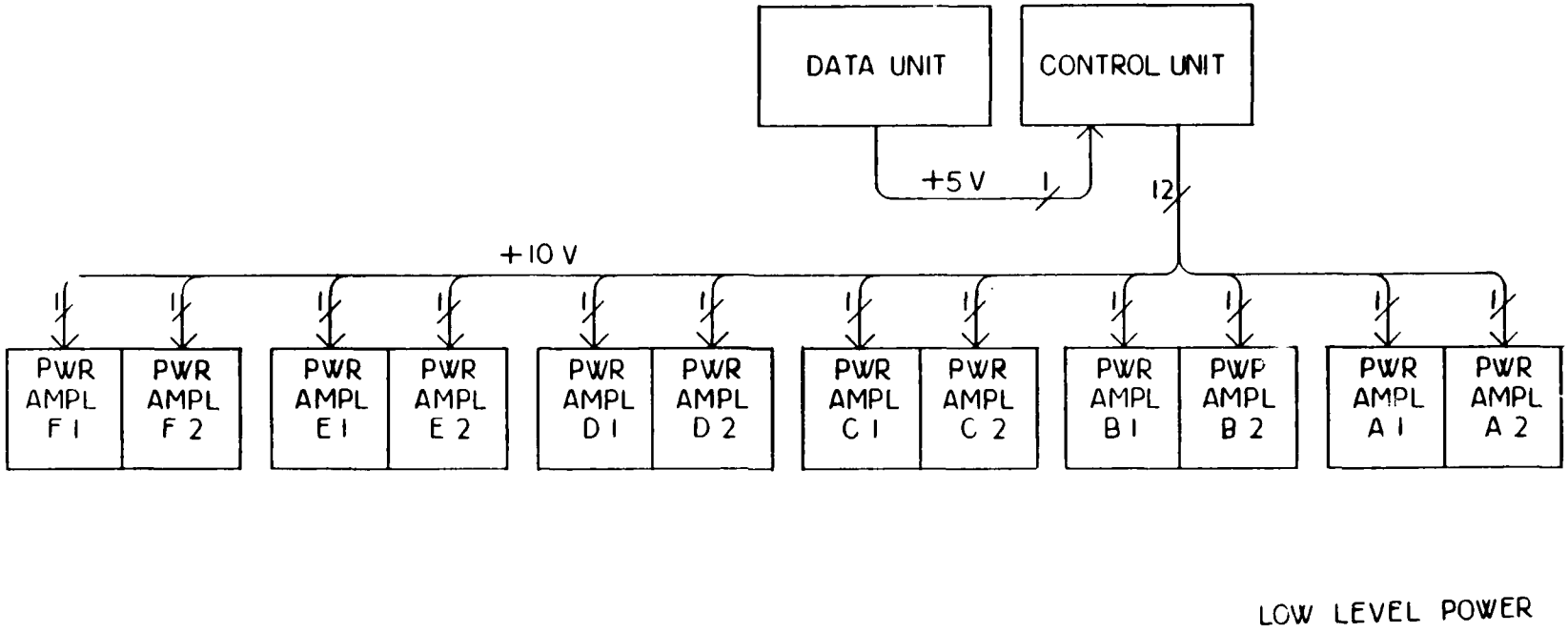

Figure 15. The Package Interconnection Diagram for the Low Level Power Circuits

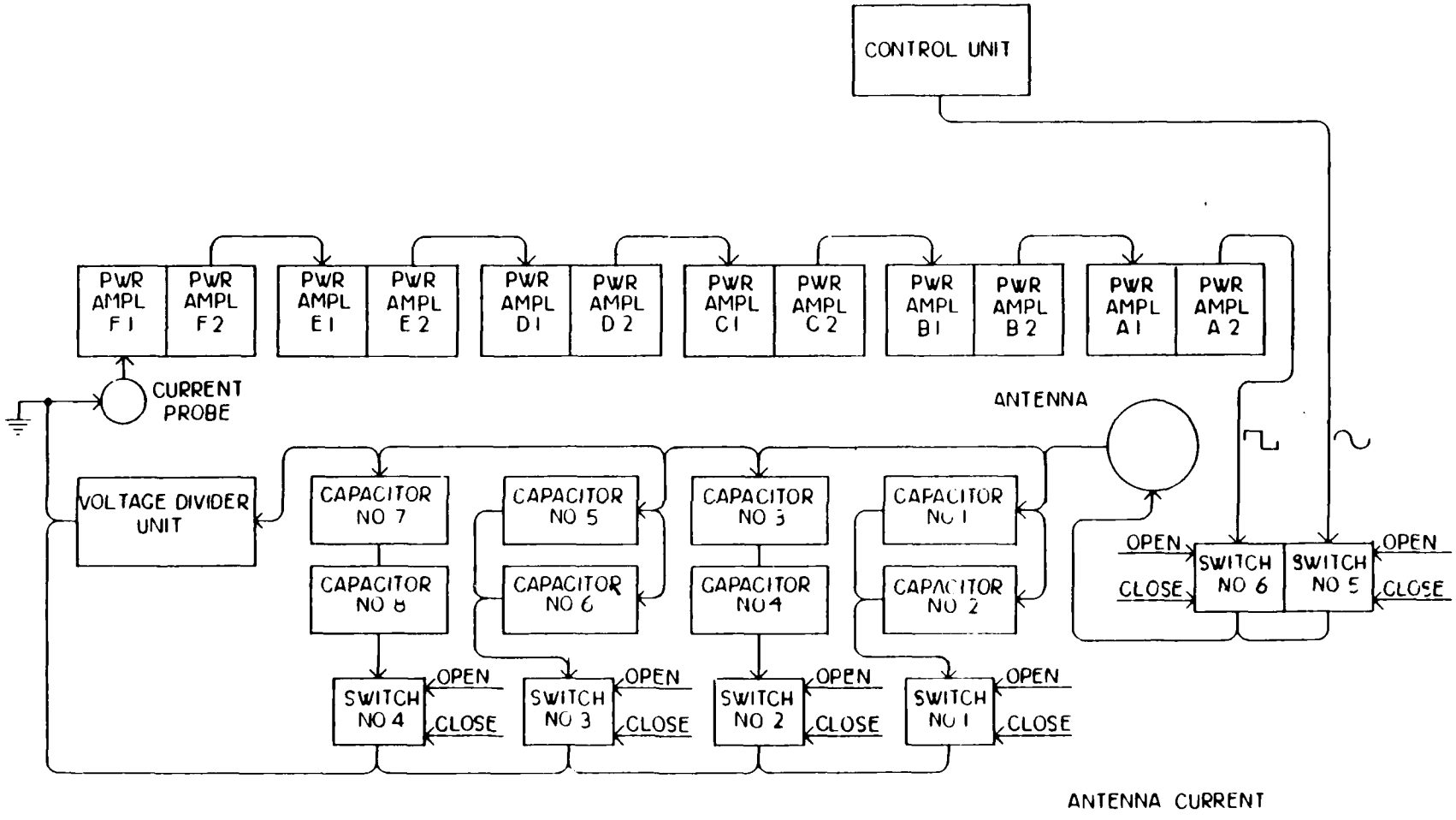

Figure 16. The Package Interconnection Diagram for the Antenna Current Circuit

Electrical Grapple Fixture for interfacing with the RMS end effector is attached to the honeycomb cylinder. Mounted on the 134 in I.D. of the honeycomb cylinder are 100 turns of 3/8 in O.D. by 1/32 in wall thickness copper tubing.

Mass Properties. The total weight of the antenna structure including reserves for growth and miscellaneous items is 2586 lbs. The detailed mass properties report is given in Appendix E.

Structural Analysis. A preliminary structural analysis was carried out on three configurations of the antenna structure subsystem. The configurations were a truss-like stucture, an octagonal configuration made out of honeycomb flat panels, and a honeycomb circular cylindrical shell. A quick structural evaluation of the truss configuration indicated several problems related to sizing of the members, and supporting the copper coils and the experiment packages. Furthermore, the rather large number of joints involved in such a design did not make the truss structure a good option. A further evaluation of the remaining two configurations with respect to ease of fabrication and placement of the copper coils and experiment packages resulted in selection of a circular cylindrical shell geometry. Antenna support point reactions were first hand computed for preliminary load factors. The results, given in Appendix F, showed that these loads were within allowable limits.

The antenna structure support point reactions for the cylindrical shell geometry were then obtained from a NASTRAN computer analysis again using the preliminary load factors. The results for an antenna location of Xo = 884.13 indicate that the longeron trunnion loads and all deflections are within the allowable limits. The keel trunnion loads exceeded the combined X-Z friction load capability governed by the aft frame strength by 496 lbs or 10% of the

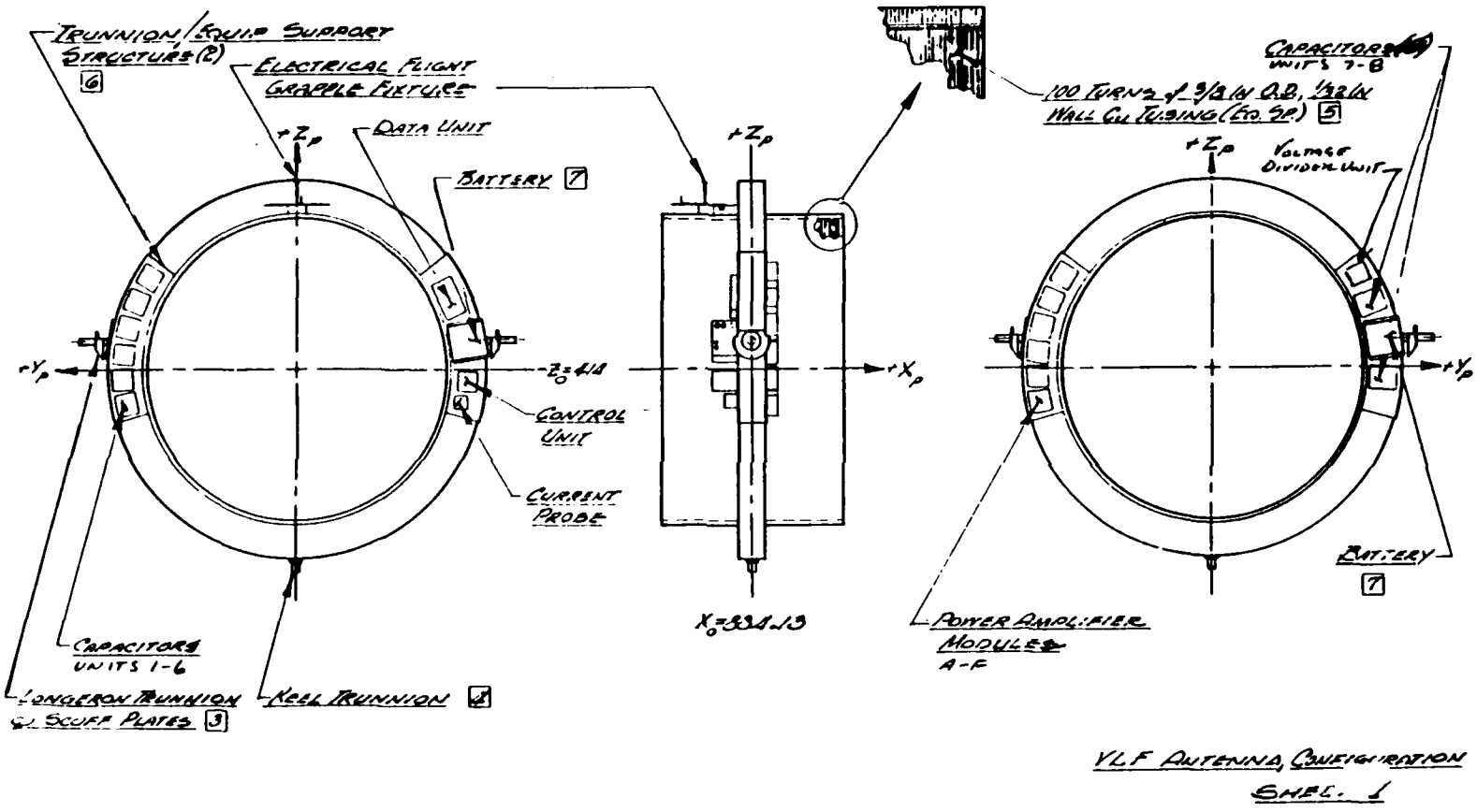

Figure 17a. The Antenna Structure

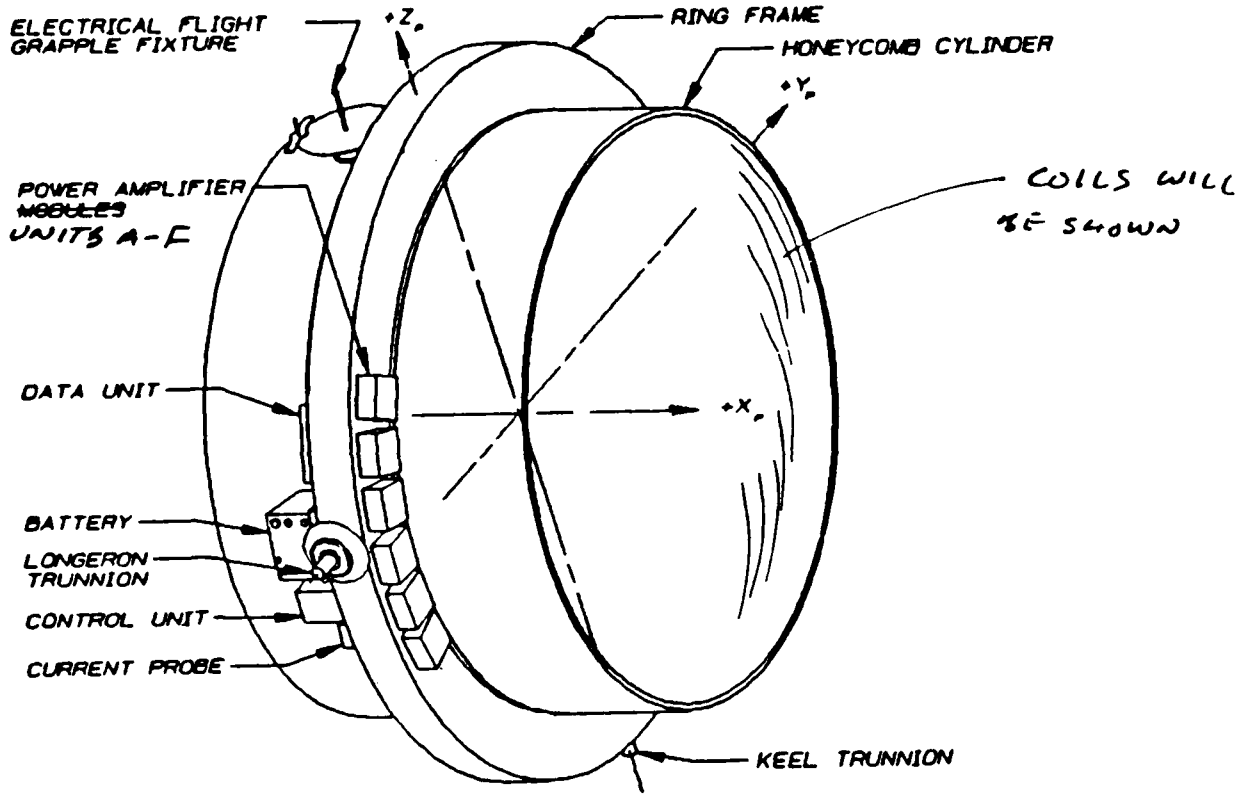

Figure 17b. The Antenna Structure

allowable load. If the antenna is relocated to Xo = 943.13, all loads are within the permissible limits. The keel X-Z friction load exceeding the allowable for the present antenna location is not a major concern since a generous allowance for the total weight exists and also the load factors used for this preliminary design were quite conservative. The attachpoint loads and deflections report is in Appendix G.

Vibration Analysis. Natural frequencies and mode shapes for the antenna structure were computed by the MATRIX computer program. Table 7 lists the frequencies under 50 Hz and their identification. The first mode (12 Hz) is a longitudinal mode, the rest are shell type modes. All of the modes were examined using an animation routine. A single frame of the animation is shown in Fig. 18. A VHS format video tape of this animation is included with the original copy of this report to NASC. The purpose of this analysis is to ensure that the antenna structure in the stowed condition meets the minimum payload frequency requirement for the Space Shuttle. The results, given in Appendix H, show that the fundamental frequency is well above the minimum requirement.

It is expected that the minimum natural frequency of the structure in the deployed condition will be higher than in the stowed condition because it is less constrained.

Stress Analysis. A stress analysis of the Antenna Structure was conducted in order to establish margins of safety for the preliminary design loads. The results are given in Appendix I. All margins of safety for the preliminary load designs are positive.

A thermostructural analysis was also conducted to obtain a conservative estimate of the thermal stresses. Again all margins of safety were positive. A

Table 7. VLF Antenna Natural Frequencies in the Stowed Condition

Mode Number	Frequency (Hz)	Mode Description
1	12.54	1st Longitudinal
2	21.37	1st Lateral
3	26.37	1st Ring Bending
4	29.36	1st Breathing
5	35.51	Shell Pitch
6	39.23	Shell Pitch
7	46.11	1st Battery Pitch

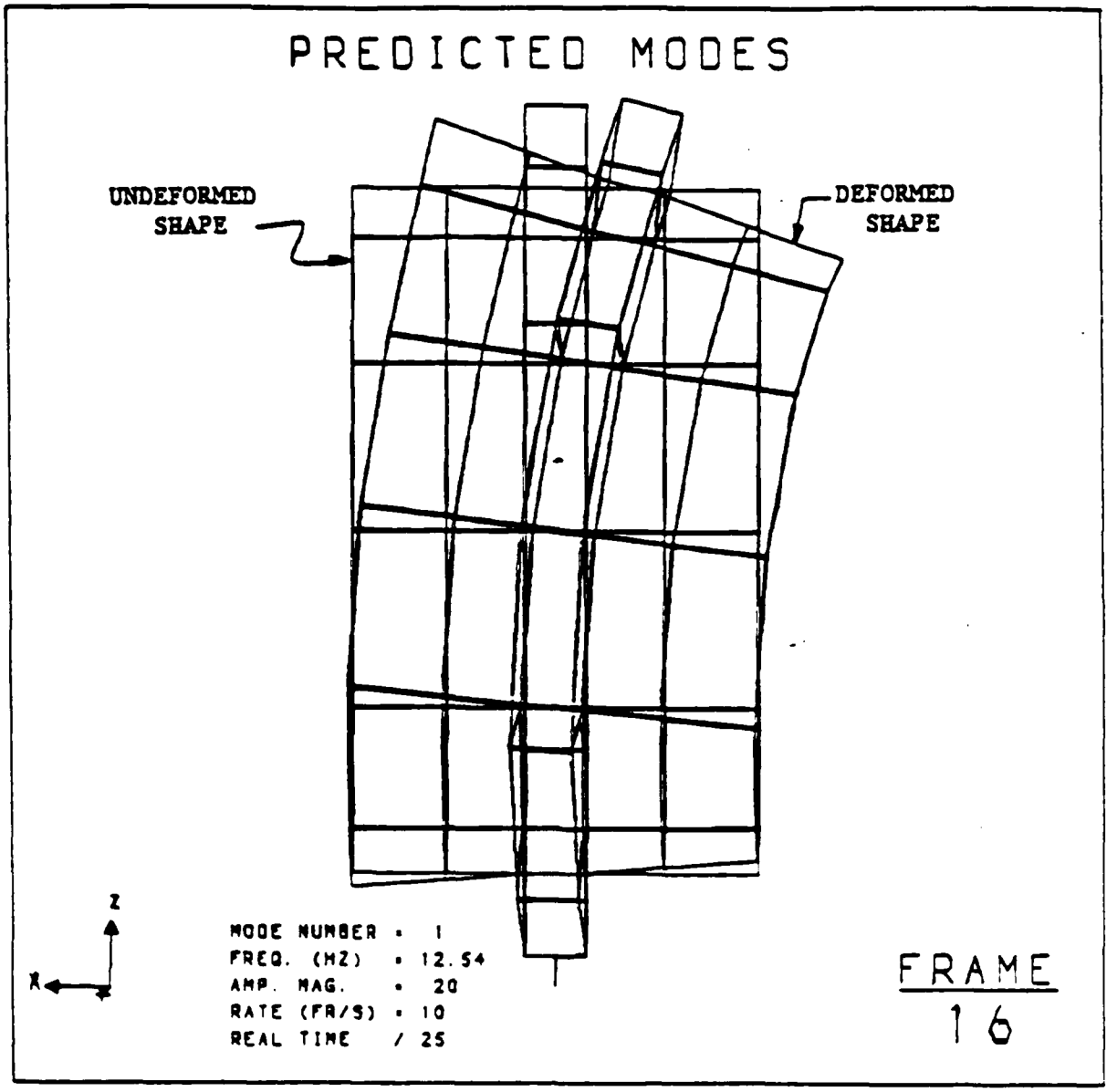

Figure 18. A Frame of the Animation from the Antenna Dynamic Model

more refined thermostructural analysis is necessary to obtain interface bonding stresses between the sandwich facesheets and the honeycomb core.

Thermal Analysis. Two of the candidate designs have been analyzed and temperature predictions made. The two designs considered are similar enough so that a single thermal analysis is applicable to both. The basic designs are cylindrical or eight sided honeycomb structures with copper tubing coiled around the perimeter in a continuous loop. The copper tubing acts as the antenna.

The thermal analysis of the antenna for the hot case assumptions shows that the maximum temperatures are 130°F and 216°F for the supporting honeycomb structure and antenna copper tubing, respectively. The cold case predictions are -115°F and -170°F for the honeycomb structure and antenna copper tubing, respectively. The hot case assumed an antenna dissipation of 2000 watts and environments of solar, earthshine, and albedo directed on the antenna from the same orientation. The cold case assumed no power dissipation and earthshine only as the external environment.

Also, preliminary temperature estimates of the electronic equipment have been made. The results appear to be too extreme under the assumptions made. It has been assumed that the equipment operates until steady-state temperatures are attained. This result in temperature predictions beyond those currently accepted as operating ranges of most common electronic equipment.

It has been proposed to consider a foamed-in-place concept to hold the 3/8 inch copper tubing, which is the essential part of the Very Low Frequency (VLF) antenna.

One of the concerns with a foamed-in-place design concept is the fact that foam is typically a low thermal conductivity material and the possibility

of overheating the tubes during operation is present. In the nominal design the copper tubing is 3,350 ft long approximately and can dissipate 2 kilowatts with a 50% duty cycle.

A worst case hot preliminary thermal analysis was performed to assess the maximum orbital temperature while the antenna is held by the RMS, outside the shuttle bay. The maximum tube temperature is about 225°F (107°C) for the worst case solar heating condition. The thickness of the foam was assumed to be 3 inches. According to the Handbook and Heat Transfer evacuated, 2 lb/ft^3, styrofoam has a thermal conductivity that appears to be acceptable. Higher density material should tend to increase the thermal conductivity.

Based on the above it is concluded that one cannot rule out the foamed-in-place concept for the VLF antenna on thermal reasons alone.

The results are given in Appendix J.

Power Subsystem

A study was performed to consider alternatives for transmitting power to the experiment at the end of the RMS. The electrical current demands of the experiment exceed the current carrying capability of the existing RMS cable. Three approaches were considered. The first did not use the RMS cable but provided a ribbon-type cable running parallel to the RMS cable or fed from a separate tension spool. Being flat, it would offer a minimum torque load on deployment and require a minimum weight and development effort. The second uses the RMS cable for transmitting power at 300 vdc. This would require an up converter at the cable input and a down converter at the output, and would limit the cable current to 9.7 amps. A similar approach would utilize an inverter as the up-converter, transmitting power at 12 kHz to a transformer

rectifier as down converter. This approach would have weight, size and efficiency benefits. The third approach would use a battery at the experiment to deliver the high current. Both primary and secondary storage systems were considered.

The third alternative using a rechargable AgZn battery is the recommended approach. A AgZn battery, EP #MAR 4544, manufactured by Eagle-Picher appears to be adequate for the experiment requirements. It contains 18-cells, and is rated at 500 ampere-hours.

Two such batteries would be used on the antenna structure. A charging circuit would be used to trickle charge the batteries at +28 vdc using the existng RMS cable.

The outline and mounting drawing for the Eagle-Picher battery is shown in Fig. 19.

Cargo Bay Packages

Two experiment packages will remain in the cargo bay during the experiment. They are the Data Interface Unit and the B-field Meter.

Data Interface Unit. The Data Interface Unit is the primary interface between the experiment and Orbiter or Space Lab pallet for command and control. It will receive commands from a Remote Acquisition Unit (RAU) in the Space Lab configuration or from a Shuttle computer and send commands via existing cables along the RMS to the Data Unit on the Antenna Structure. It will also receive data via existing cables along the RMS from the Data Unit and send this data to the RAU or Shuttle computer. The Data Interface Unit will be based on the same digital architecture as the Data Unit and will have the same physical configuration. The outline and mounting drawing for the Data Interface Unit is shown in Fig. 4.

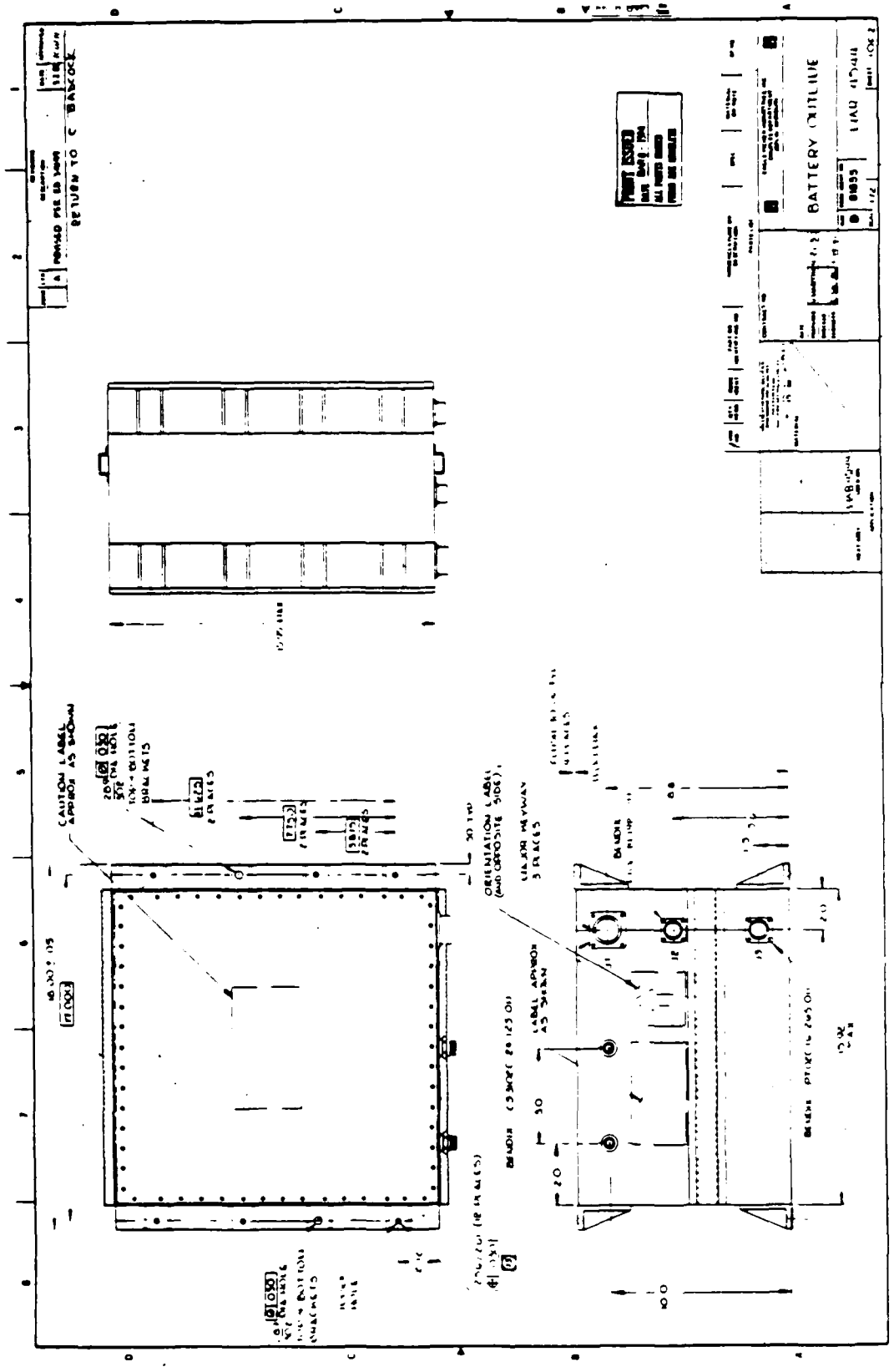

Figure 19. The Outline and Mounting Drawing for the Eagle-Pitcher Battery

B-Field Meter. The B-field Meter will make a three axis measurement of the a.c. magnetic field generated by the current flowing in the elf antenna coil. This measurement will be used to monitor the performance of the antenna in real time and to verify the current levels and modulation schedule for the transmitter during data reduction and analysis.

The circuit used for the B-field meter will be similar to the circuits used for the elf/vlf receiver described below.

The outline and mounting drawing for the B-field Meter is shown in Fig. 20. The three axis antenna system is not shown. It will either be a set of orthogonal air-core loop antennas or ferrite-core antennas. The antenna system will fit inside a 24 in sphere.

Subsatellite Packages

The primary measurement made by the experiment is the measurement of the field intensity of the transmitter at distances from 10 to 100 km from the transmitter. This measurement must be made by a subsatellite equipped with an elf/vlf receiver.

ELF/VLF Receiver. The elf/vlf receiver will measure the three components of the electric field and the three components of the magnetic field at the signal frequency of the transmitter. The receiver will have six separate 32-step spectrum analyzers with fully synthesized local oscillators. A block diagram of one of the analyzers is shown in Fig. 21. The receiver can operate in either a stepping mode or can be tuned to a fixed frequency. The bandwidth of each channel will be 100 Hz. The instrument will have three dynamic ranges. The entire dynamic range is 100 dB. Table 8 shows the dynamic range of the SFR at each of the three attenuation settings.

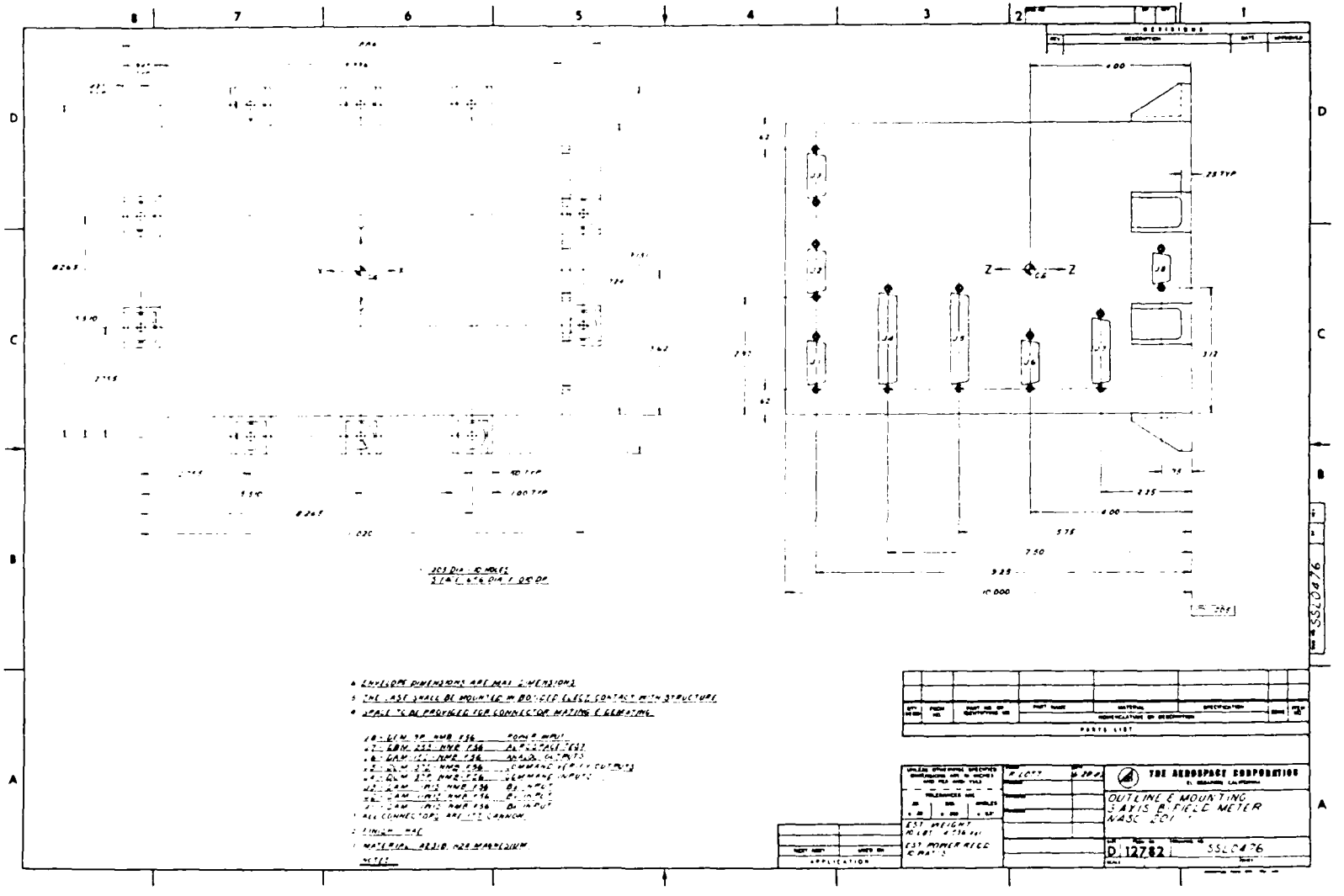

Figure 20. The Outline and Mounting Drawing for the B-Field Meter

STEPPED FREQUENCY RECEIVER INPUT

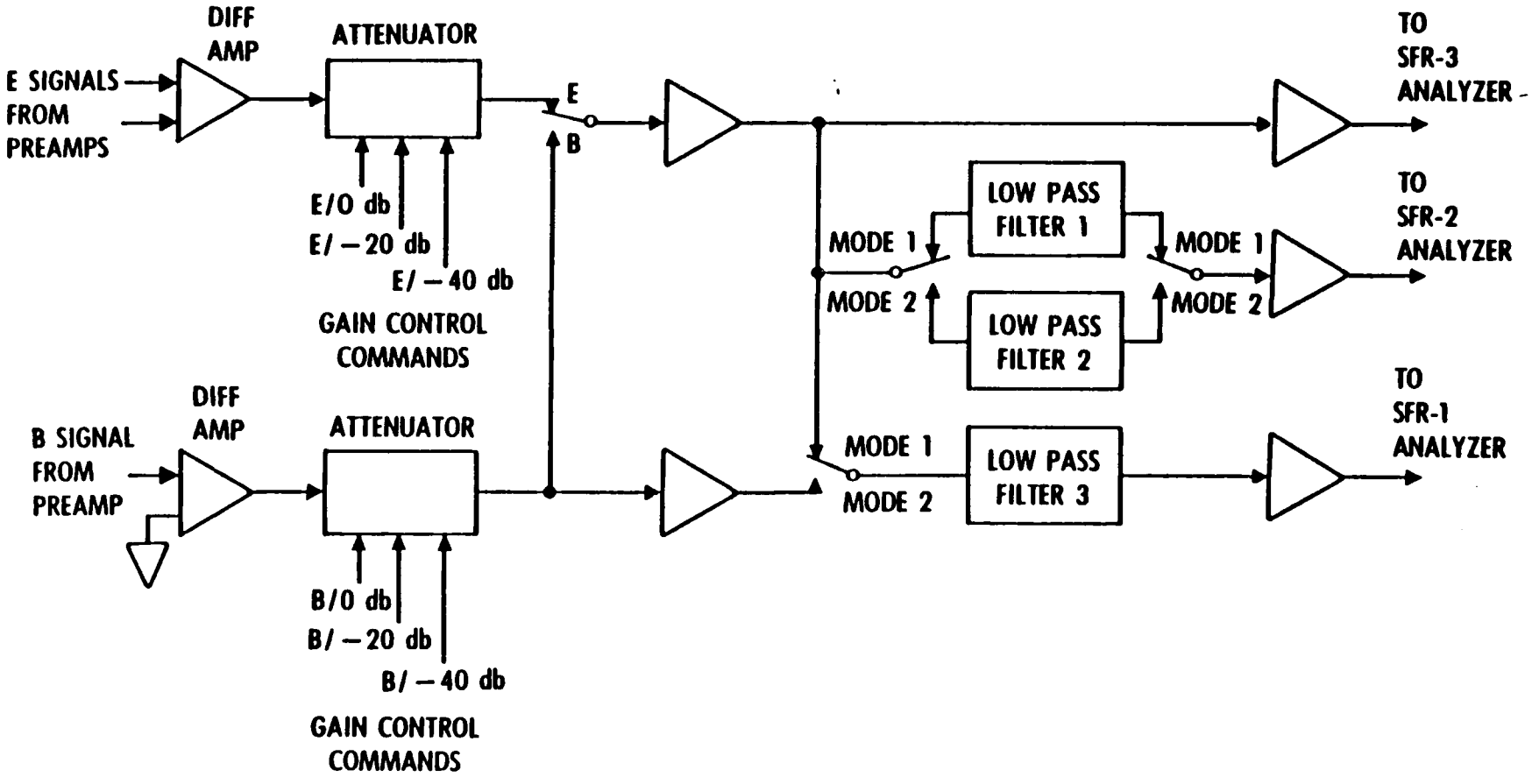

Figure 21a. A Block Diagram of One of the Stepped Frequency Receiver Analyzers

STEPPED FREQUENCY ANALYZER
ONE OF THREE

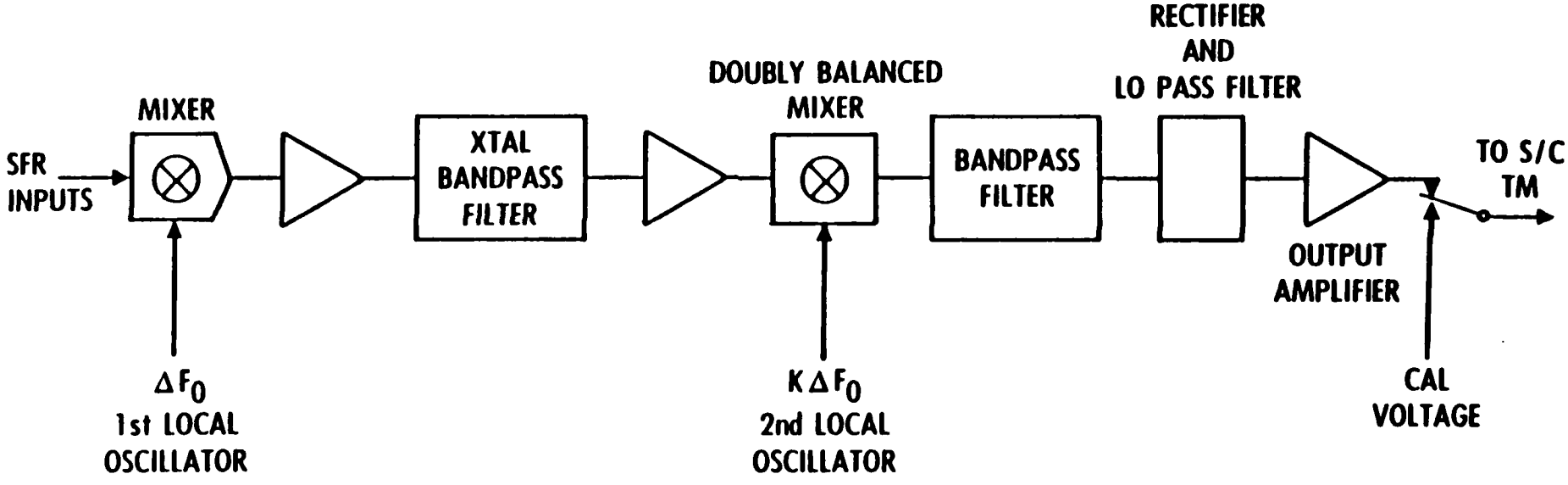

Figure 21b. A Block Diagram of One of the Stepped Frequency Receiver Analyzers

Table 8. Dynamic Range of the SFR at Each of the Three Attenuation Settings

Antenna	Attenuation		
	0 dB	-20 dB	-40 dB
E-field	10 μV - 10 mV	100 μv - 100 mV	1 mV - 1 V
B-field	0.0316 - 31.6 pT	0.316 - 316 pT	3.16 pT - 3.16 nT

The receiver will also have a broadband channel capable of telemetering the entire spectrum from 100 Hz to 20 kHz. This channel can be tuned to either the electric or the magnetic antenna and is used to determine the characteristics of the background noise. Background noise will be due to lightning generated sferics and whistlers and to natural emissions from the particles and plasmas in the ionosphere and magnetosphere.

The characteristics and requirements for the NASC-201 elf receiver as they were defined for the RPDP spacecraft are defined in Appendix K.

AMPTE-IRM VLF/MF Receiver. A prototype of the stepped frequency reciver designed for the NASC-201 experiment has been built and flown aboard the AMPTE-IRM spacecraft. This work was supported in part by the Office of Naval Research and in part by the U.S. Air Force Systems Command through MOIE funding at The Aerospace Corporation.

The primary objective of the AMPTE experiment was to study the interaction between an artificially injected cold plasma and the natural flowing space plasmas. The SFR measures the intensity and spectra of electromagnetic and electrostatic waves that result when a cold, dense Lithium or Barium plasma interacts with the hot, rapidly flowing, natural plasmas such as the solar wind and magnetosheath plasmas. The experiment employed two antennas to detect the electromagnetic and electrostatic emissions, a ferrite core search coil antenna and a 42-m tip-to-tip electric dipole antenna. The AMPTE SFR consisted of one package with three channels. The channels covered three separate frequency ranges: 0.2-2.5 kHz, 0.9 to 9 kHz, and 9 to 99 kHz.

The AMPTE spacecraft was launched on August 16, 1984. The receiver was turned on and checked out shortly after injection into the final orbit. The SFR is working perfectly and the vehicle has a very low EMI level on the

electric antenna. There is a moderate EMI level on the magnetic antenna because the ferrite core antenna is mounted on a very short mast. A sample spectrogram from the first lithium release is shown in Fig. 22.

The success of this experiment has provided a flight qualification for the receiver to be used on the subsatellite as part of the NASC-201 experiment.

A more detailed description of the stepped frequency receiver flown aboard AMPTE is given in Appendix L.

Environmental Sensors. The following environmental sensor measurements are required from other experiments aboard the subsatellite: electron density and temperature, ion composition and temperature, and d.c. magnetic field. One second resolution is required of these measurements. These physical parameters are required to evaluate the plasma dispersion relations for wave modes that can be excited by the antenna in the ionosphere. They control the antenna pattern and the propagation of the waves through the plasma.

Antenna System. A three axis antenna system is required for both the electric and the magnetic fields. Since such an antenna system has a major impact on the design of the vehicle, it is not practical to provide a detailed design at this stage in the definition of the subsatellite.

The magnetic antennas will typically fit within a 24 in. sphere and should be mounted at least 3 m from the body of the spacecraft. The electric antenna should consist of orthogonal dipole elements at least 10 m from tip-to-tip. The length of the dipole should significantly exceed the size of the major axis of the vehicle.

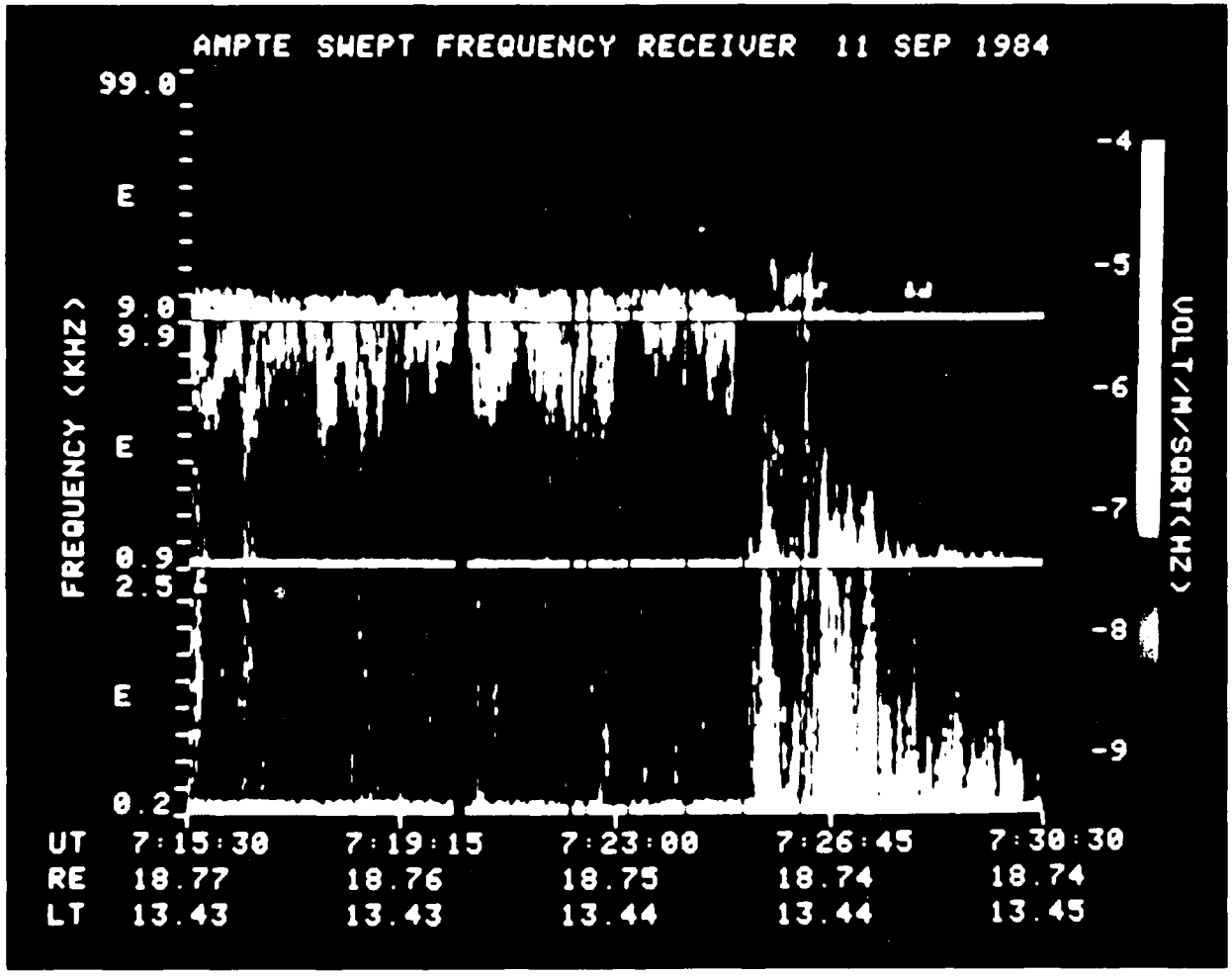

Figure 22. A Sample Spectrogram from the First Lithium Release by the AMPTE-IRM Spacecraft

ELECTRICAL PERFORMANCE

A computer code was developed to predict the performance of the solenoidal antenna. The physical parameters chosen as the baseline for the antenna coil are given in Table 9.

A typical printout showing the parameters that must be considered is shown in Table 10. The typical performance predicted by this code is given in Table 11. The values of the current and voltage expected are somewhat smaller than given there. They are dependent upon the losses specified for the circuit elements. Plasma losses will further reduce the current and voltage for the assumed power. The magnetic moment predicitons were based only on circuit losses. Plasma losses were not considered.

Electromagnetic Interference

The antenna current produces large a.c. induction magnetic fields around the antenna coil. Computations were performed to determine if the a.c. magnetic field was within allowable payload limits within the cargo bay. The results are shown in Fig. 23. In that figure the shuttle emissions are plotted as a function of frequency as a dashed line and the payload allowable limit is plotted as a solid line.

The field intensity from the coil is indicated as a function of distance from the axis of the coil along the vertical line at 4,000 Hz. The field is below the allowable limit if the axis of the coil is 15 m above the cargo bay.

LABORATORY MEASUREMENTS

In order to test this concept for an antenna in a plasma, a one-third scale-model loop antenna was operated in a 5-m diameter space plasma simula-

Table 9. The Physical Parameters Chosen as the Baseline for the Antenna Coil

Coil Description:	
Diameter to center of conductors (to fit inside a 134 in. dielectric structure)	133.625 in.
Height	81 in.
Coil weight	466 lb. (copper only)
Coil material	3/8 in. soft copper refrigeration tubing
Turns	100
Conductor spacing, centers	0.807 in.
Gap between conductors	0.43 in.
Inductance	0.032 Henrys

Table 10. Antenna Electrical Characteristics

11	16-Mar-84		
12		Standard	
13	POWER BUDGET PARAMETERS	Antenna	
14	Power Available Watts	300	NASC-201 Solenoidal Antenna
15	Delivery Efficiency	0.85	
16	Power to Amplifier Watts	2550	
17	Amplifier Efficiency	0.9	
18	Power to Antenna Circuit Watts	2295	
19			
20	MECHANICAL CHARACTERISTICS		
21	Coil diameter, in.	134.0 in.	
22	Coil diameter-cm	340.36 cm	
23	Coil height, ft	6.75 ft	
24	Coil height, cm	205.74 cm	
25	Coil height, in.	81	
26	Coil weight, gr	212000 gr	
27	Coil weight, lb	466 lb	
28	Tubing diameter, in.	0.375 in.	
34	Conductor length, cm	107074 cm	
35	Turns	100 turns	
36	Conductor length, ft	3513 ft	
37	Number of 50 ft coils	70 coils	
38	Spacing, cm	2.055 cm	
39	Spacing, in.	0.809 in.	
40	Gap positive?? in.	0.43 in.	
72	ELECTRICAL PARAMETERS		
73	Inductance Henrys	0.032 Henrys	
74	Impedance, ohms	199 ohms	
75	Q factor	170 Q	
76	Bandwidth, Hz	5.9 Hz	
77	Capacity to tune, farads	8.01E-07 farads	
78	Estimated capacity, farads	9.00E-07 farads	
79	Ratio	1.1230	
80			
81	Capacitor Dissipation factor	0.002	
82	ESR for diss. factor, ohms	0.3972 ohms	
83	Capacitor lead resistance	0.025 ohms	
84	Capacitor, total ESR	0.4222 ohms	
85	ESR + coil resistance, ohms	1.5919 ohms	
86	Circuit Q	125 Q	
87	Power available watts	2295 watts rms	
88			
89	OPERATING PARAMETERS		
90	Frequency, Hz	1000 Hz	
91	Current, amps rms	38.0 amps	
92	Series voltage, rms	60.4 volts	
93	Input resistance, ohms	1.592 ohms	

Table 10. Antenna Electrical Characteristics (Continued)

94	Capacitor k-volts rms	7.54 k-volts
95	MAGNETIC MOMENT-AMP-M SQUARED	34,594 A-M Sq
96		
97	POWER DISTRIBUTION, COIL AND CAPACITORS	
98	Capacitor electric loss, watts	572.6 watts
99	Capacitor lead loss, watts	36.0 watts
100	Total power loss in capacitors	608.7 watts
101	Coil power dissipation, watts	1686.3 watts
102	Total power loss, watts	2295 watts

Table 11. Magnetic Moment Predicted for the Magnetic Dipole Antenna

Frequency	500 Hz	1000 Hz	2000 Hz	4000 Hz
Tuning Capacitor	3.2 uF	0.8 uF	0.2 uF	.05 uF
Capacitor Voltage	4000 V	8000 V	16,000 V	32,000 V
Circulating Current	40 A	40 A	40 A	40 A
Magnetic Moment	40,900 Amp/m^2	38,500 Amp/m^2	34,000 Amp/m^2	28,300 Amp/m^2

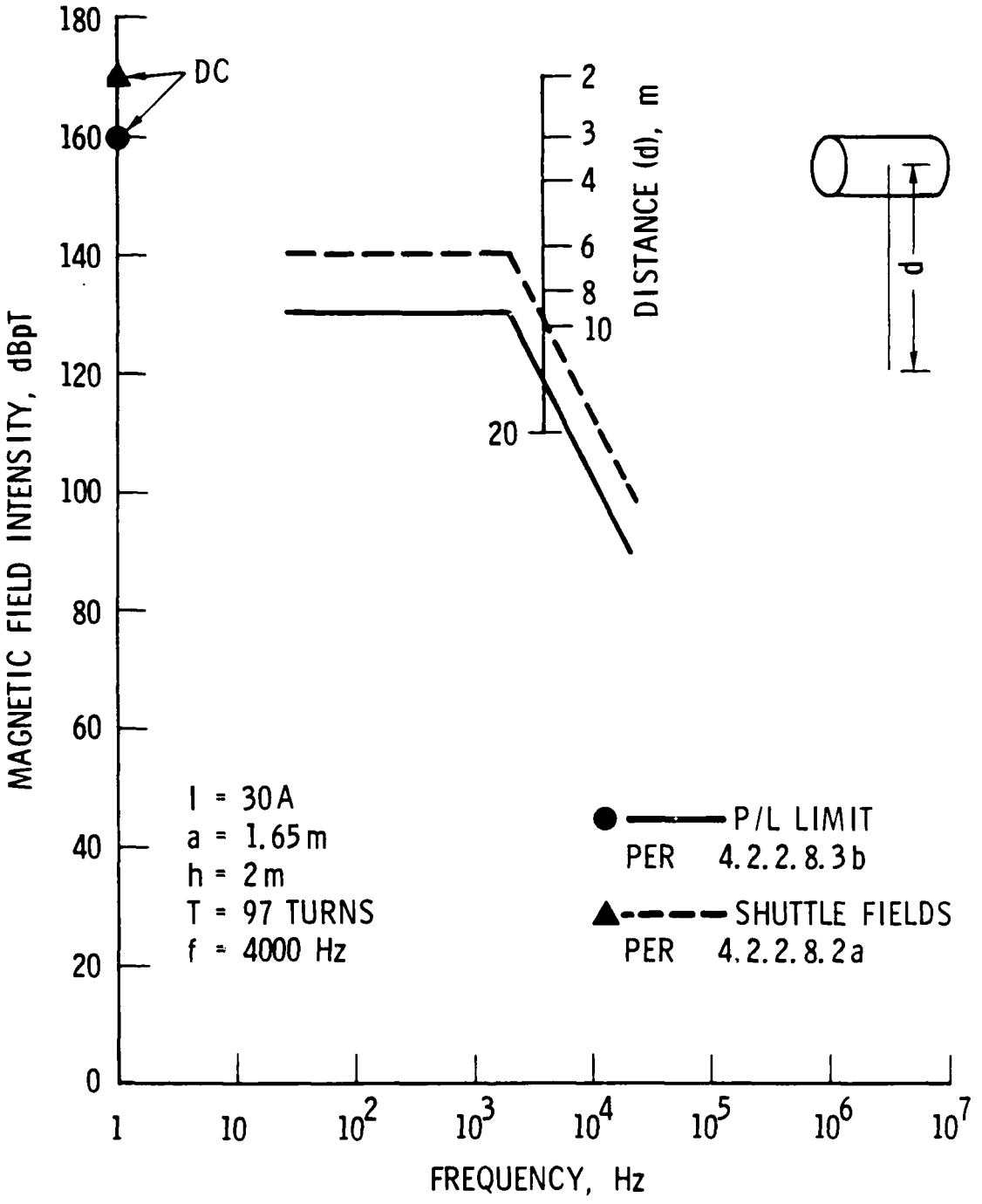

Figure 23. Magnetic Field Intensity Around the Elf Antenna

tion chamber at the NASA Lewis Research Center. The antenna parameters are listed in Table 12. The objectives of the test were to measure the absolute value of the complex impedance, the resonant frequencies, and the near fields of the antenna. The thermal properties of the structure and plasma instabilities generated by the VLF fields were also measured.

The measurements were made in an argon ion plasma under two conditions. A relatively uniform density of 8×10^4 elec/cm^3 was produced using four plasma guns. A higher density of 1.2×10^6 elec/cm^3 was produced at the antenna by augmenting the plasma guns with a plasma thruster at one end of the chamber. The thruster produced a directed flow along the axis of the chamber with a density gradient of 10^6 elec/cm^3/m. The electron density and temperature were measured by four Langmuir probes placed about the antenna. In the low density plasma the electron temperature was 1.1 eV. In the high density plasma the temperature was 0.6 eV. Helmholtz coils provided a 0.4 G field parallel to the axis of the cylindrical vacuum chamber.

Plasma Chamber Results

One of the major results of the measurements was the confirmation that the resonant frequency of the tuned antenna circuit is insensitive to the plasma density. Fig. 24 shows typical resonances in the antenna current for the antenna in the plasma. These measurements were made by sweeping the frequency at a constant amplifier voltage. Below a plasma wave instability threshold a smooth curve is obtained. Above that threshold, which occurs at an antenna current of 8.6 A r.m.s. in Fig. 24, the circuit resistance abruptly increases. There is only a slight shift in the resonant frequency. Even in the absence of the plasma the resonant frequency depends upon the orientation of the antenna in the tank. The resonant frequency is slightly lower when the

Table 12. Scale-Model Antenna Parameters

Diameter	110 cm
Height	66 cm
Weight	60.5 kg
Copper Tubing	3/8 in O.D.
Turns	37
Structural Material	Lexan

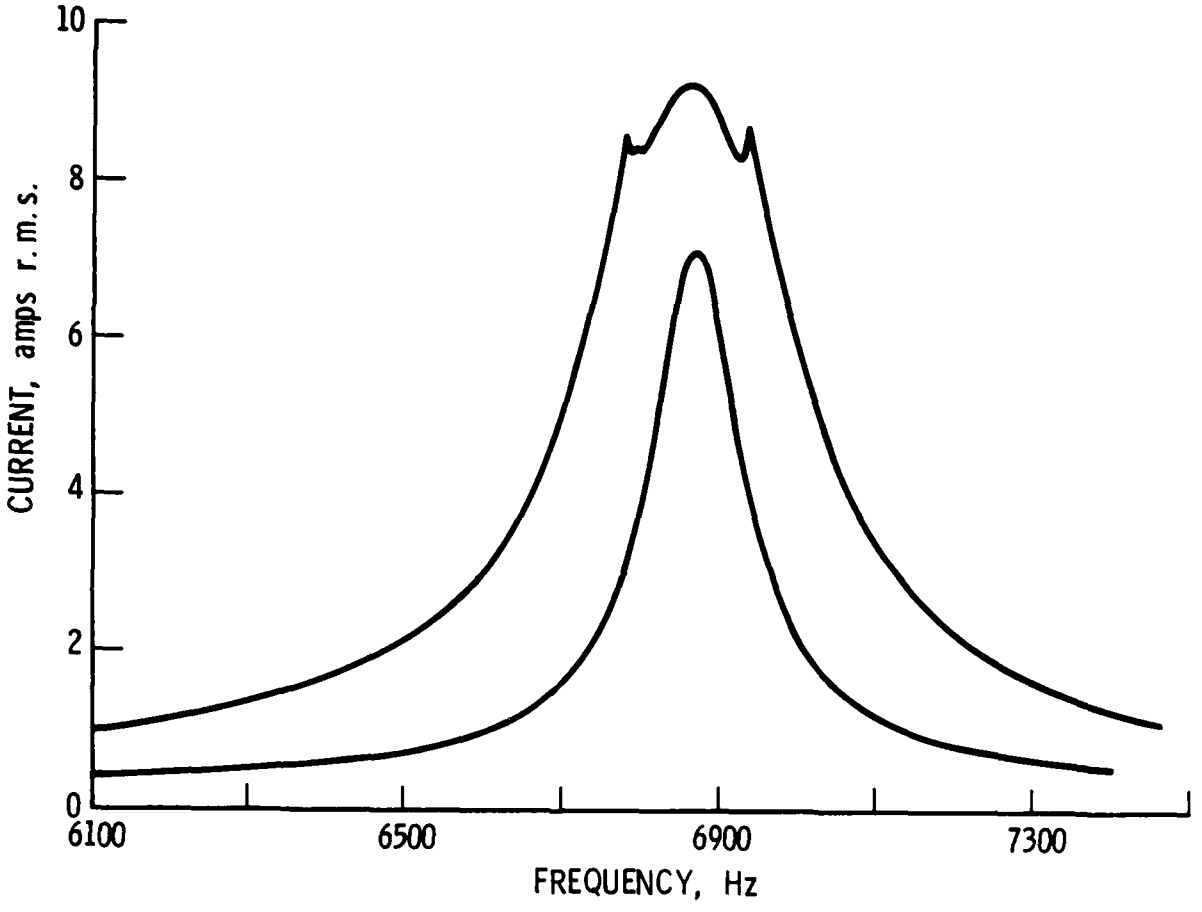

Figure 24. Antenna Current as a Function of Frequency at Two Voltage Drive Levels

axis of the antenna is perpendicular to the axis of the tank. At 500 Hz the shift in the resonant frequency is smaller than the resolution (~ 5 Hz) of the measuring instruments over the entire range of plasma densities and antenna orientations. At 7000 Hz there is a shift of about 20 Hz or 3 parts in 10^3 at the highest density.

The a.c. magnetic field component of the near field was measured by small search coils at several locations about the antenna. The near magnetic field was directly proportional to antenna current and independent of the plasma density as expected from Ampere's law in Maxwell's equations.

The results are summarized as follows:

1. The resonant frequency of the antenna circuit was insensitive to the plasma density.
2. The series resistance of the circuit increases in the plasma. This increase is small below 1 kHz and large above 3 kHz. The increased resistance is attributed to power lost to plasma turbulence.
3. The intensity of the ac magnetic-field component in the near field of the antenna in the plasma is unchanged from its value in free space as expected.
4. The impedance of the antenna is insensitive to the rotation angle with respect to the dc magnetic field. In particular no significant impedance variations occurred at angles of 0 and 90°.

These tests confirm that a full size antenna can be tuned using fixed capacitance. The losses to be expected from plasma turbulence with the full size system cannot be readily extrapolated from the scale model tests. In particular the voltage across the terminals of the full size antenna will be significantly larger than the voltages across the terminal of the model.

A report with the results from these measurements is given in Appendix M.

END

4-87

DTIC